Earth Sciences
2022; 11(5): 232-249
http://www.sciencepublishinggroup.com/j/earth
doi: 10.11648/j.earth.20221105.11
ISSN: 2328-5974 (Print); ISSN: 2328-5982 (Online)

Petrography and Geochemistry of Metasedimentary Rocks from the Southwestern Portion of the Yaoundé Group in Cameroon: Provenance and Tectonic Implications

Victor Metang[1, *], Bernard Tassongwa[2], Rose Ngo Belnoun[1], Henri Appolinaire Kenzo[1], Myrianne Tawo Toussi[1], Diane Marilyn Nkamga Mbakam[1], Lea Grace Tene Kengne[1], Legrand Joseph Tchop[1, 3], Lucas Mouafo[1], Jean Pierre Tchouankoue[1]

[1]Department of Earth Sciences, Faculty of Science, University of Yaounde I, Yaounde, Cameroon

[2]Department of Earth Sciences, Faculty of Science, University of Dschang, Dschang, Cameroon

[3]Instituearch, Buea, Cameroon

Email address:

metangvictor@yahoo.fr (Victor Metang)

[*]Corresponding author

To cite this article:

Victor Metang, Bernard Tassongwa, Rose Ngo Belnoun, Henri Appolinaire Kenzo, Myrianne Tawo Toussi, Diane Marilyn Nkamga Mbakam, Lea Grace Tene Kengne, Legrand Joseph Tchop, Lucas Mouafo, Jean Pierre Tchouankoue. Petrography and Geochemistry of Metasedimentary Rocks from the Southwestern Portion of the Yaoundé Group in Cameroon: Provenance and Tectonic Implications. *Advances in Materials*. Vol. 11, No. 5, 2022, pp. 232-249. doi: 10.11648/j.earth.20221105.11

Received: August 9, 2022; **Accepted**: August 25, 2022; **Published**: September 5, 2022

Abstract: The tectonic evolution and provenance of the sediments from the Yaoundé Group remain poorly understood and somewhat enigmatic although the information it has already provided. This work presents the results of integrated field mapping, petrography and whole-rock geochemical studies of less documented metasedimentary rocks cropping in the southwestern portion of the Yaoundé Group, with the aim to enhance the geological setting of this group. These metasedimentary rocks comprise garnet-bearing chlorite schists, garnet micaschists and kyanite-bearing garnet migmatites. Their mineral assemblages suggest prograde metamorphism, from greenschist to granulite through amphibolite facies. Whole-rock geochemical data reveals wide range of Fe_2O_3 + MgO + TiO_2 contents, from 7.3 to 32.6 wt.%, due to the diversity of lithological units. High Ba (616.833 ppm), V (145.333 ppm) and Zr (227.591 ppm) values suggest continental crust source materials. The average ratios of Nb/Ta (15.25), Zr/Hf (36.52) and Y/Ho (27.41) are closer to those of the upper continental crust. The average Th/U ratio, above 4.0 in investigated metasedimentary rocks, indicates intense weathering in the source areas or sediment recycling. The protoliths of the rocks are post-Archean shales and greywackes deriving mostly from andesites and granodiorites, probably from of the Congo craton and/or the Adamawa-Yadé block. The prominent tholeiitic geochemical affinity of these rocks suggests their emplacement in an active margin context and/or oceanic island arc setting.

Keywords: Yaoundé Group, Metasedimentary Rocks, Upper Continental Crust, Active Margin, Congo Craton

1. Introduction

The Yaoundé Group belongs to the Central African Orogenic Belt [52, 77, 42, 59, 58, 82, 47, 50]. They are bordered by the Congo craton or Ntem Complex in the south (Figure 1) and the Central Domain or Adamawa-Yade Group in the north [77, 74, 25, 26, 5, 49]. Bordered in the west by the Central Cameroonian Shear Zone, it extends eastward into the Central African Republic [26]. Many interesting works have been published in the region, notably the pioneering works of Nzenti et al. [52] that support the hypothesis of an epicontinental basin of a passive margin. Toteu et al. [78] formulated the hypothesis of a peri- or intracratonic continental basin that closes following the convergence of the Adamawa-Bafia and Congo craton units involving northward subduction. Mvondo et al. [45] also proposed an intracratonic model that indicates the burial of the Yaoundé Group by the Adamawa-Yadé formations followed by the exhumation of

migmatites accompanied by flakes of ultrabasic rocks probably from the upper mantle along the planes of deep listric faults. In an effort to understand the Yaoundé Group, Nkoumbou et al. [50] demonstrated that the Yaoundé basin is likely the expression of extensional processes in the northern Congo craton that guided rifting, shattering and limited oceanization. In line with Nkoumbou et al. [50], Fuh et al. [20] explained that the Boumnyebel island arc setting extends eastward up to Yaoundé, and probably up to Lomié in the southeastern Cameroon. Besides, these authors added that the best model to understand the context is the south-north subduction of the Pan-African Yaoundé hot oceanic crust under the Archean Adamawa-Yade block. Despite these numerous works, the emplacement context of the protoliths of the Yaoundé Group metasediments is still under debate due to the lack of large-scale petrographic mapping and geochemical studies, which are key elements to answer this regional preoccupation. This paper aims at determining the source and depositional environment of the protoliths of these metasediments using petrographic and geochemical features of the Mbalmayo, Bikok, Mbankomo, Makak and Matomb formations.

2. Geological Setting

In Cameroon, the Central African Orogenic Belt presents three main domains [77, 50, 74, 25, 26, 46, 5, 49]: the northern domain, the central or Adamawa-Yade domain and the southern domain.

The northern domain extends along the western edge of Cameroon, and into Poli [76] and Mayo Kebi regions, SW of Chad [61]. It consists of: (i) metasediments (greywackes, carbonate argillites, iron argillites) and metavolcanites (830 Ma; U/Pb age on metarhyolites zircon, [75]); (ii) a gneissic (amphibole, biotite and garnet gneiss) and amphibolite assemblage alternating with retromorphosed granulite bands (800-900°C, 13-14 kb) [8] associated with a tectono-metamorphic history related to Palaeoproterozoic granulite units (2100 Ma; U/Pb age on zircon, [60]) all crosscut by diorites, granodiorites and calc-alkaline tonalites dated at 630 Ma (U/Pb age on zircon, [75]); (iii) Neoproterozoic orthogneisses whose petrography and geochemistry are compatible with a continental arc domain associated with a subduction zone [9].

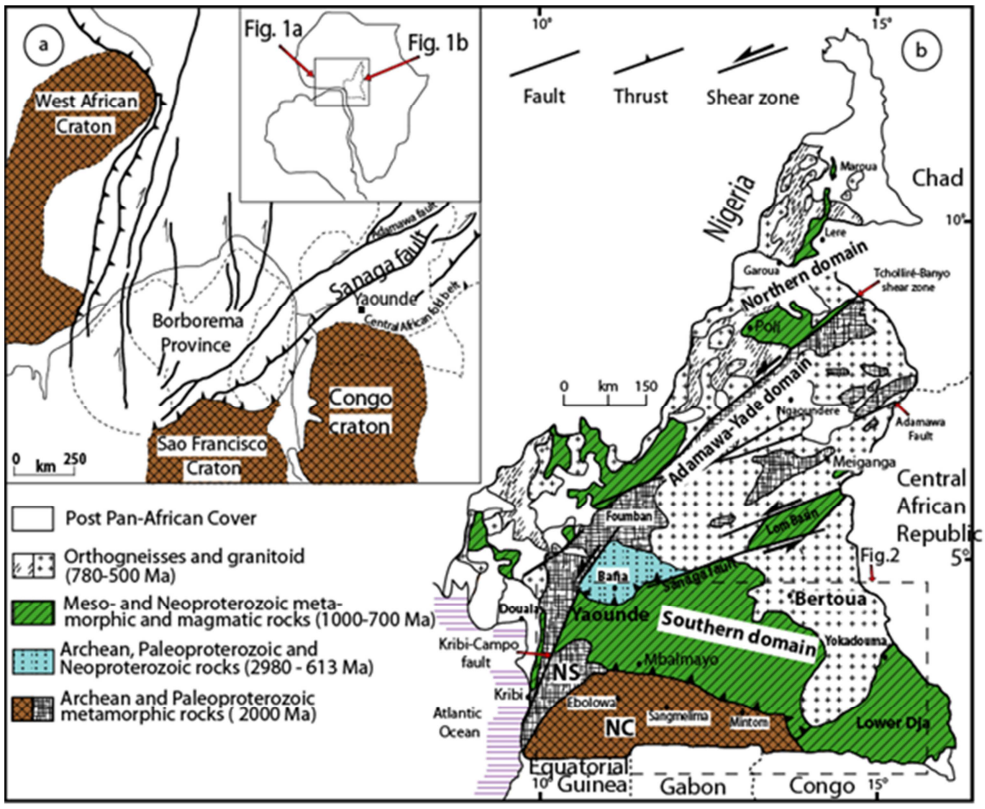

Figure 1. *The Pan-African Belt of Central Africa: (a) continent scale geodynamic reconstruction [54]; (b) main subdivisions in Cameroun (modified from [74].*

The central or Adamawa-Yade domain, located between the Tcholliré Banyo Fault in the north and the Sanaga Fault in the south [74], covers the Central Cameroon area, southern Chad and northern part of Central Africa [21, 23, 73]. Pan-African metadiorites (637±5 Ma to 608 ± Ma; U-Pb age on zircon, [23]), scattered in the Adamawa-Yade domain (Central Africa) and in the Borberema province (NE Brazil), show tectono-metamorphic evolution in the Ediacaran. The geological formations of the Central Cameroon domain exposed in the Mbé – Sassa-Mbersi region, represents the exhumed mid-to lower part of the former orogenic root of the Pan-African Central Africa Orogenic Belt that underwent partial melting, lateral flow and intrusion of mafic to felsic calc-alkaline magmas between 650 and 580 Ma [68]. Post-collisional Pan-African granites such as those of Batié consist of biotite granites and amphibole granites, emplaced between 630 and 547 Ma during the

transitional period between the crustal thickening (ca. 630-610 Ma) and the development of shear zones, first sinistral (610-580 Ma) and then dextral movements (585-540 Ma), and exhumed in a transpressive dextral NE-SW strike-slip tectonic setting [31]. The crustal evolution of the Adamawa-Yade domain, suggests an Archean/Paleoproterozoic microcontinent broken away in early Neoproterozoic [74]. The pre-Pan-African history includes Meso to Neoarchean crustal accretion and associated magmatism prior to Paleoproterozoic events, west of the Central African Orogenic Belt [22].

The southern domain or the Yaoundé Group [43, 52] is limited by the central domain in the north, the Congo Craton or Ntem Complex in the south, the Kribi Kampo Fault in the west and continues eastward into the Central African Republic in the Bolé and Gbaya series [62]. The metasedimentary rocks are less than 700 Ma with a distinct local Eburnean (~2.0 Ga) and Tonian-Cryogenian (~1.0 - 0.7 Ga) sources [58]. This domain comprises the Yokadouma, Ayos-Mbalmayo-Bengbis and Yaoundé series. The Yokadouma series contains interstratified basalt flows with a pillow lava deposit typical of subaqueous effusion contemporary with sedimentation [80]. The basic magmatism of continental tholeiite composition, reveals a pre-Pan-African intracontinental extension at the northern edge of the Congo Craton [80, 79]. The Ayos-Mbalmayo-Bengbis series extends above 500 km along the northern edge of the Congo Craton and in the Central African Republic in the Bolé series [43] with four facies: chlorite micaschists, aluminous micaschists, muscovite quartzites and chlorite quartzites. In the north, the Ayos-Mbalmayo-Bengbis schists lay under the aluminous micaschists of the Yaoundé series [43], whereas in the south, the contact is straightened with the Congo craton [11]. Petrographic and chemical features are of a sedimentary, detrital, clay-carbonate series metamorphosed in greenschist facies or amphibolite facies conditions. The Yaoundé series presents mainly two lithological units: (i) a metasedimentary unit of garnet and kyanite gneiss, garnet and plagioclase gneiss and garnet micaschists with levels of calcium silicate rocks, and interspersed quartzites and talcschists, (ii) a meta-igneous unit of pyriclasites, pyroxenites, metadiorites, metagabbros and talcschists [52, 82, 20, 38]. New LA-ICP-MS zircon U-Pb geochronology indicates partial melting crystallization at 595 ± 4 Ma for the in-source granodiorite leucosomes [38]. These granodiorite leucosomes derive from the partial melting of metadiorites during a period of intense migmatization in the Yaoundé group [50, 38]. The metamorphic paroxysmal conditions were 650°-850°C and 9.5-12kb [43, 48, 82, 59]. The protolith of garnet and kyanite migmatites corresponds to a clay-carbonate sedimentary sequence (pelites, greywackes, dolomites and evaporates) with interstratified basic volcanic bands [3, 52, 69].

3. Methodology

Nine garnet-bearing chlorite schists (Grt-Chl schists), four garnet micaschists (Grt micaschists) and eleven kyanite-bearing garnet migmatites (Ky-Grt migmatites) samples were selected for whole-rock geochemical analysis at the Bureau Veritas Commodities Canada Ltd (Acme Lab), Vancouver (Canada). Major elements compositions were determined by X-ray fluorescence (XRF) using the pulp, while trace and rare earth elements (REE) compositions were determined by inductively coupled plasma-mass spectrometry (ICP-MS). For major elements, samples were fused with lithium metaborate-lithium tetraborate flux which also includes an oxidizing agent (Lithium Nitrate), then poured into a platinum mold. The resultant disk was analyzed by XRF spectrometry in conjunction with a loss-on-ignition at 1000°C. Data from both determinations were combined to produce a "total" weight percentage. For trace elements, samples were added to lithium metaborate/lithium tetraborate flux, well mixed and fused in a furnace at 1025°C. The resulting melt was cooled and dissolved in an acid containing nitric, hydrochloric and hydrofluoric acids, and analyzed by ICP-MS. The accuracy of the analysis varies for major elements (0.1%-0.04%), trace elements (0.1-0.5%) and REE (0.01-0.5 ppm). STD SO-19 standard was used and data quality assurance was established by applying it as unknown between samples. In addition, two samples were analyzed in duplicate to gauge the accuracy of measures. The discrepancy among duplicates is below 0.5 wt.%. The REE analytical precision is at 5% for concentration >10 ppm and 10% when lower. The analytical data are reported in table 1.

4. Field Observations and Petrography

Field observations and petrographic studies carried out on three main metasedimentary rocks of the Yaoundé Group show: Grt-Chl schists in the south in contact with the Congo craton, Grt micaschists on Grt-Chl schists, and Ky-Grt migmatites above Grt micaschists in the north (Figure 2). The modal abundance was estimated from the area percentage chart (Using the International Union of Geological Science) based on nineteen Grt-Chl schists, twenty-one Grt micaschists and twenty-five Ky-Grt migmatites samples.

4.1. Grt-Chl Schists

Grt-Chl schists outcrop in slabs (Figure 3a) or blocks along streams. Blocks up to 10 m height are scattered. On a macroscopic scale, three petrographic facies are defined according to the garnet sizes: coarse-grained, medium-grained and fine-grained facies. Oriented and centimetric quartz boudins (Figure 3b) occur in some outcrops. Microscopic observations show lepidogranoblastic texture with chlorite (60-70%), amphibole (5-10%), quartz (5-8%), garnet (3-5%), plagioclase (2-3%), biotite (0.5-1%), muscovite (0.5-1%), alkali feldspar (0.1-0.5%), calcite (0.1-0.5%) and accessory opaque minerals and epidote. Chlorite forms continuous or discontinuous layers with biotite lamellae (Figures 3c and 3d), that sometimes surround clusters or quartz exudates. Chlorite lamellae (≤ 2 mm) are allotriomorphic, associated with quartz. In places chlorite flakes are folded (Figure 3d). Chloritisation of biotite is common. Amphibole porphyroblasts present a spindle-shaped habitus with quartz or plagioclase inclusions and a corroded edge (Figure 3e) transforming into biotite or chlorite. Quartz rarely appears as isolated grains, but as concentric exudates (Ø < 1 mm) or

sigmoidal pockets surrounded (Figure 3e) by phyllite minerals (chlorite, biotite and muscovite). These small sigmoidal lenses sometimes occupy the core of microfolds (Figures 3c and 3e). Plagioclase occurs as isolated crystals (Figure 3f), or a mosaic of crystals (0.064 mm) sometimes around well-developed plagioclase blasts and often associated with epidote granules. Fissured porphyroblasts show corrosion and epidote intergrowth associated with sericite probably from sericitized plagioclase (albite). Some porphyroblasts undergo rim to core chloritization. Garnet is subhedral to euhedral, or helicitic with shadow zones constituted of recrystallized quartz, biotite, muscovite and chlorite. Sigmoidal or spiral inclusions of quartz and opaque minerals are present (Figure 3g). Biotite (≤ 0.03 x 0.08 mm) is less abundant, with inclusions of zircon (Figure 3h) and opaque minerals. Muscovite, chlorite and biotite form lepidoblastic layers bearing quartz (Figure 3c) or, rarely, amphibole and plagioclase. Subhedral to euhedral alkali feldspar is rare, associated with quartz and plagioclase and biotite inclusions. The millimetric-sized calcite (Figure 3f) appears as isolated prisms probably resulting from the transformation of amphibole.

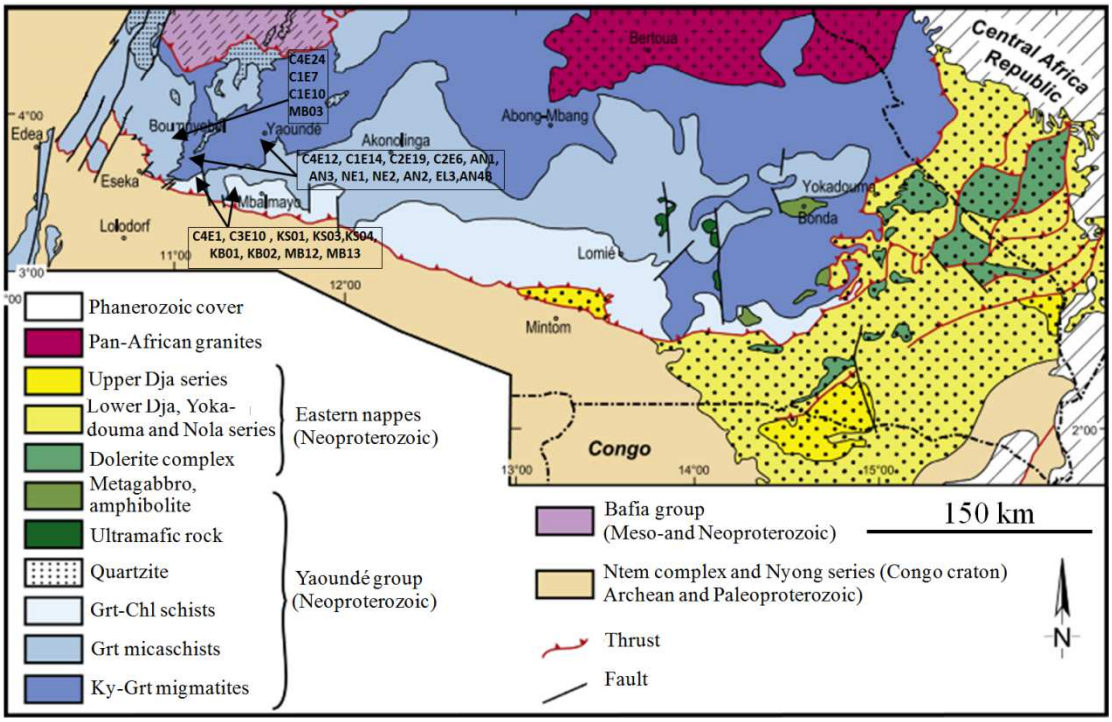

Figure 2. *Sketch of the geological map of the Pan-African formations near the Congo Craton (after [11, 80, 78, 50] and location of sampling sites.*

4.2. Grt Micaschists

Grt micaschists outcrop in slabs and domes (Figure 4a) or in decimetric to metric blocks on hillsides or along river beds (Figure 4b). On hillsides and along streams, micaschist blocks are associated with quartzite blocks. They are generally multi-metric in talwegs and metric on ridges and slopes. At road cuts, light grey quartzofeldspathic bands of centimetric size alternate with dark grey bands of centimetric to decimetric size rich in muscovite. Banding is wavy, boudined and intercalated with centimetric to metric levels of amphibolites (Figure 4c). Quartzofeldspathic minerals are sometimes boudined (~ 5 x 30 cm). The accumulation of metric to decametric blocks of Grt micaschists create caves of several meters deep in places. Overall, the size of garnet (Figure 4d) and the abundance of muscovite indicate five petrographic facies: light coarse-grained garnet facies with a folded layer of variable thickness (5 - 20 cm), dark facies with medium-sized garnet and variable thickness (10 - 30 cm), white millimetric garnet facies with less than 6 cm thickness, large muscovite flakes and fine garnet grains facies, and small muscovite flakes and coarse garnet grains facies. Grt micaschists present a granoblastic to granolepidonematoblastic texture (Figure 4e) with quartz (25-30%), muscovite (15-20%), biotite (15-20%), garnet (10-12%), plagioclase (7-8%), alkali feldspar (2-4%), amphibole (1-2%), kyanite (1-2%), chlorite (1-2%) and accessory minerals (sphene, zircon and opaque minerals). Quartz in grains (≤ 190 x 110 µm) and bands (1200 µm) follows schistosity, and is associated with muscovite, biotite and opaque minerals. Biotite and muscovite lamellae surround sigmoid lenses of quartz exudates (Figure 4f). Millimetric biotite and muscovite lamellae develop in pressure shadows of sigmoid lenses. Muscovite occurs as stretched lamellae (1 x 1.2 mm) strongly folded following the schistosity; it surrounds quartz and garnet porphyroblasts. Pockets of muscovite flakes and small quartz crystals sometimes scatter, surrounded by muscovite and biotite porphyroblasts up to 2 mm long. Anhedral lamellae of biotite (<1.2 mm) shows inclusions of zircon; it alters into muscovite (Figure 4g). Opaque minerals concentrate along biotite cleavages. Small biotite lamellae recrystallize at pressure shadows of rotated crystals such as garnet (Figure 4g) and sigmoid lenses of quartz crystals (Figure 4f). Plagioclase (1.5 mm) is rare and anhedral with biotite inclusions. The

saussuritization of some porphyroblasts results in subhedral grains of epidote (Figure 4e). Anhedral to subhedral porphyroblasts of alkali feldspar (Figures. 4e and 4g) not exceeding 1 mm and displaying biotite and muscovite inclusions. Amphibole is either scattered in the rock or forms millimetric layers miming schistosity (Figure 4h). The presence of rare, scattered and oriented kyanite (Figures. 4e and Figure 5a) suggests a high grade amphibolite facies. Chlorite lamellae (1.6 x 0.56 mm) are subhedral (Figure 5b). Garnet in anhedral to subidiomorphic crystals (3 mm) sometimes presents irregular crown (Figure 5a) made of quartz, alkali feldspar, biotite. Biotite and muscovite are in inclusions. Garnet presents brownish weathering mark along cracks (Figure 5b).

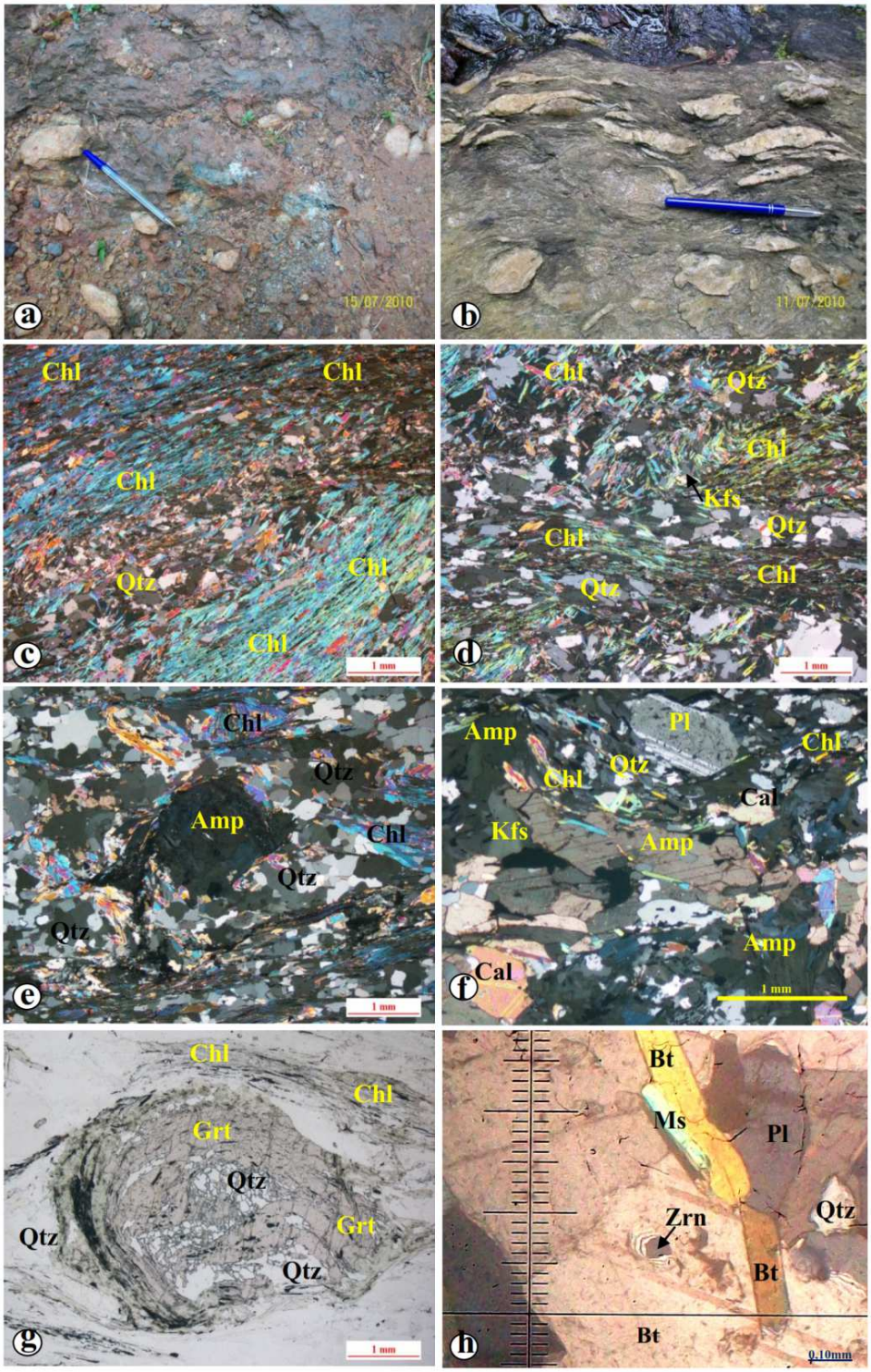

Figure 3. *Photographs and microphotographs of Grt Chl Schists: (a) Slab of Grt chlorite schists; (b) Grt chlorite schist with quartz boudins; (c) Chlorite layers embedding the quartz lenses; (d) Folded chlorite layers alternating with quartz levels; (e) Amphibole porphyroblast with corroded edges; (f) Plagioclase and calcite crystals in the matrix; (g) Helicitic garnet crystals with sigmoidal or spiral inclusions; (h) Zircon inclusion in biotite.*

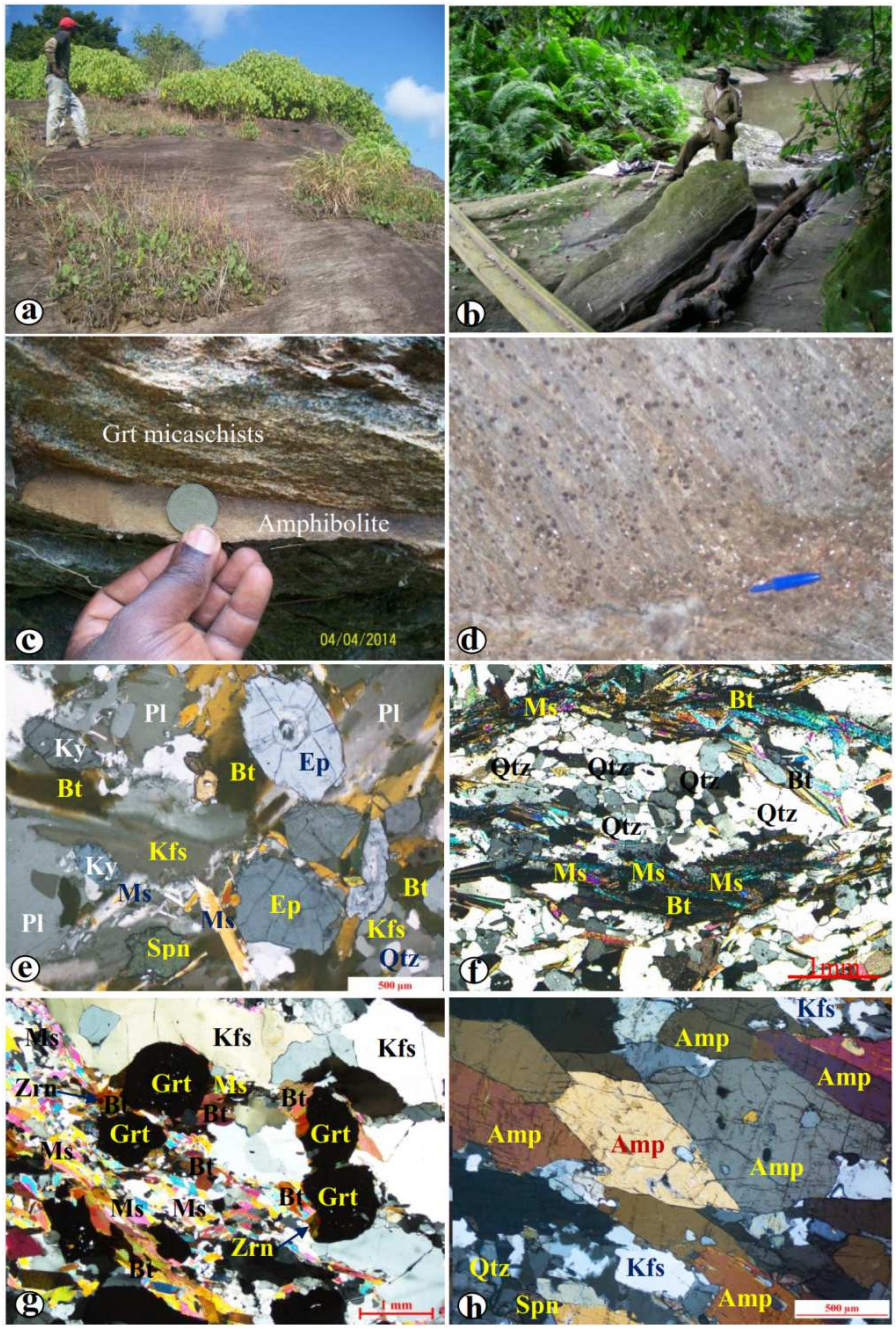

Figure 4. *Photographs and microphotographs of Grt micaschists: (a) Micaschist dome; (b) Grt micachists blocks along a river; (c) Amphibolite intercalation in Grt micaschists; (d) Coarse-grained garnet in micaschists; (e) Heterogranular granolepidonematoblastic texture in Grt micaschists; (f) Muscovite and biotite surrounding a quartz lens; (g) Mixed biotite and muscovite layers; (h) Millimetric layers of euhedral amphibole crystal in Grt micaschists.*

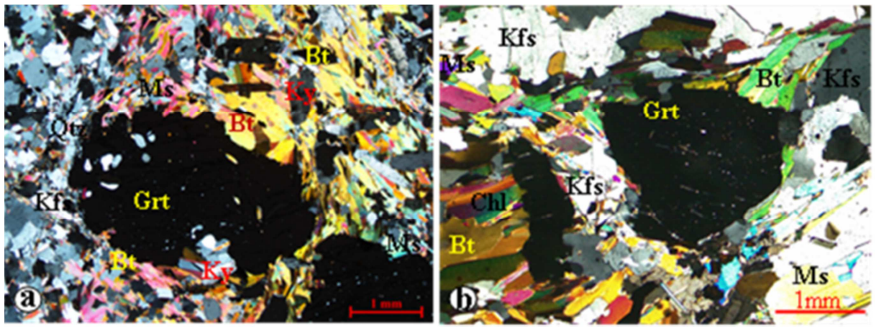

Figure 5. *Microphotographs of Grt micaschists: (a) Garnet crystal with irregular edges and inclusions of biotite and quartz; (b) Garnet porphyroblast weathering along cracks.*

4.3. Grt-ky Migmatites

Grt-ky migmatites outcrop as Grt-Chl schists and micaschists (Figures. 6a and 6b). In addition, the other migmatite features are nebulites (muscovite and biotite clusters, Figures. 6c and 6d), arterites (mainly garnet and biotite facies, Figures. 6e and 6f), embrechites (lens-shaped feldspar migmatites, Figs. 6g and 6h), sigmoidal quartz-feldspar boudins (Figure 7a) and oriented kyanite crystals (Figure 7b), and traces of partial melting showing migmatization (Figure 7c). The rocks present a granolepidonematoblastic texture (Figure 7d-h) with quartz (15-20%), biotite (10-15%), muscovite (10-15%), plagioclase (10-15%), garnet (9-10%), orthoclase (6-7%), amphibole (4-5%), microcline (1-3%), kyanite (1-2%), epidote, calcite, sphene and opaque minerals.

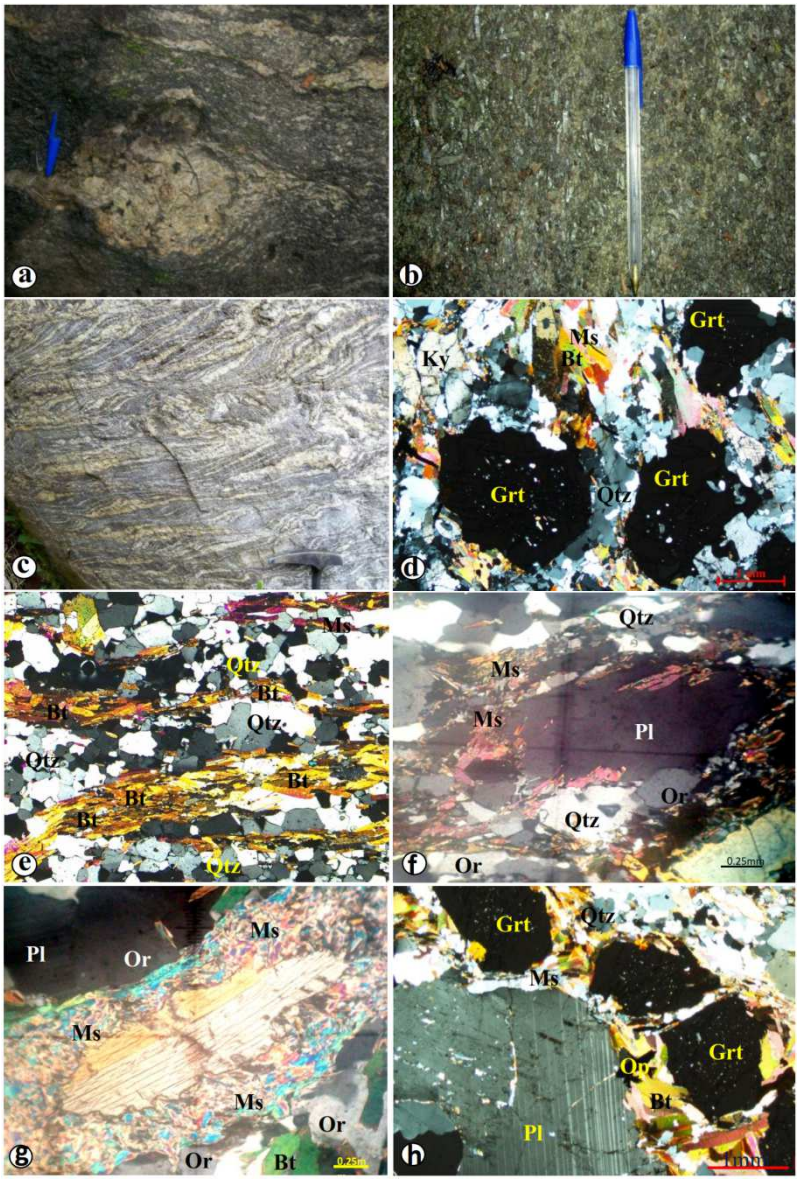

Figure 6. *Photographs and microphotographs of Grt-Ky migmatites: (a) Dome; (b) Blocks; (c, d) Hand specimen and thin section of muscovite and biotite clusters; (e, f) Hand specimen and thin section of garnet and biotite facies; (g) Lens-shaped feldspar.*

Quartz is in grains (0.16 x 0.08 mm) or polycrystalline interlocked bands (0.5 x 0.12 mm) with crystals of phyllite (0.02 mm) and feldspar in the interstices. Biotite and muscovite surround quartz exudates, evidence of intense folding of quartz veins. Neoformed blasts are associated with biotite and muscovite at the level of pressure shadows due to the rotation of some garnet porphyroblasts (Figure 7d). Biotite is in subidiomorphic lamellae (≤ 1 mm). In nebulites, biotite and muscovite form clusters (Figure 6d). In arterites, they form millimetric and discontinuous layers. In embrechites, biotite flakes in smaller sizes surround feldspar patches. In garnetites, biotite is generally in the interstices of garnet grains (Figure 6f). Zircon and opaque inclusions are common. Muscovite and biotite form lepidoblastic layers that alternate with granoblastic layers rich in quartzofeldspar minerals (Figure 7e). Muscovite lamellae (1 mm) are anhedral to subhedral. Small lamellae

result from the retromorphose of plagioclase (Figure 7f) and kyanite (Figure 7g). Juxtaposed lamellae form rosette-like textures. Porphyroblasts are embedded in small quartzofeldspathic and phyllite layers. Plagioclase occurs in large anhedral to subhedral patches (0.5 x 2 mm, Figure 7h) showing weathering features. The symplectic (myrmekitic) texture is characterized by recrystallized quartz veinlets in plagioclase (Figure 8a). The patches with dark green epidote-bearing mixture indicate saussuritization. Amphibole is anhedral to subhedral (1.1 x 1.8 mm) with serrated or corroded contours. The centripetal chloritization of porphyroblasts reflects retromorphosis, giving biotite lamellae and millimetric epidote grains. Garnet (0.5-1mm) in allotriomorphic to subidiomorphic crystals is cracked with a snowball texture and quartz inclusions (Figure 7d and 7f). Quartz bands associated with opaque minerals most often outline the internal schistosity in garnet porphyroblasts (Figure 8b). Secondary biotite develops along garnet cracks (Figure 8b). Orthoclase is associated with quartz; both form felsic layers (Figures. 8c and 8d). Microcline is rare with an unclear grid pattern in large (≤ 1.2 mm) subhedral patches inclosing quartz (Figure 8c). Leucosome levels are rich in quartzofeldspathic minerals with locally oriented biotite and/or muscovite flakes (Figures. 8c and 8d).

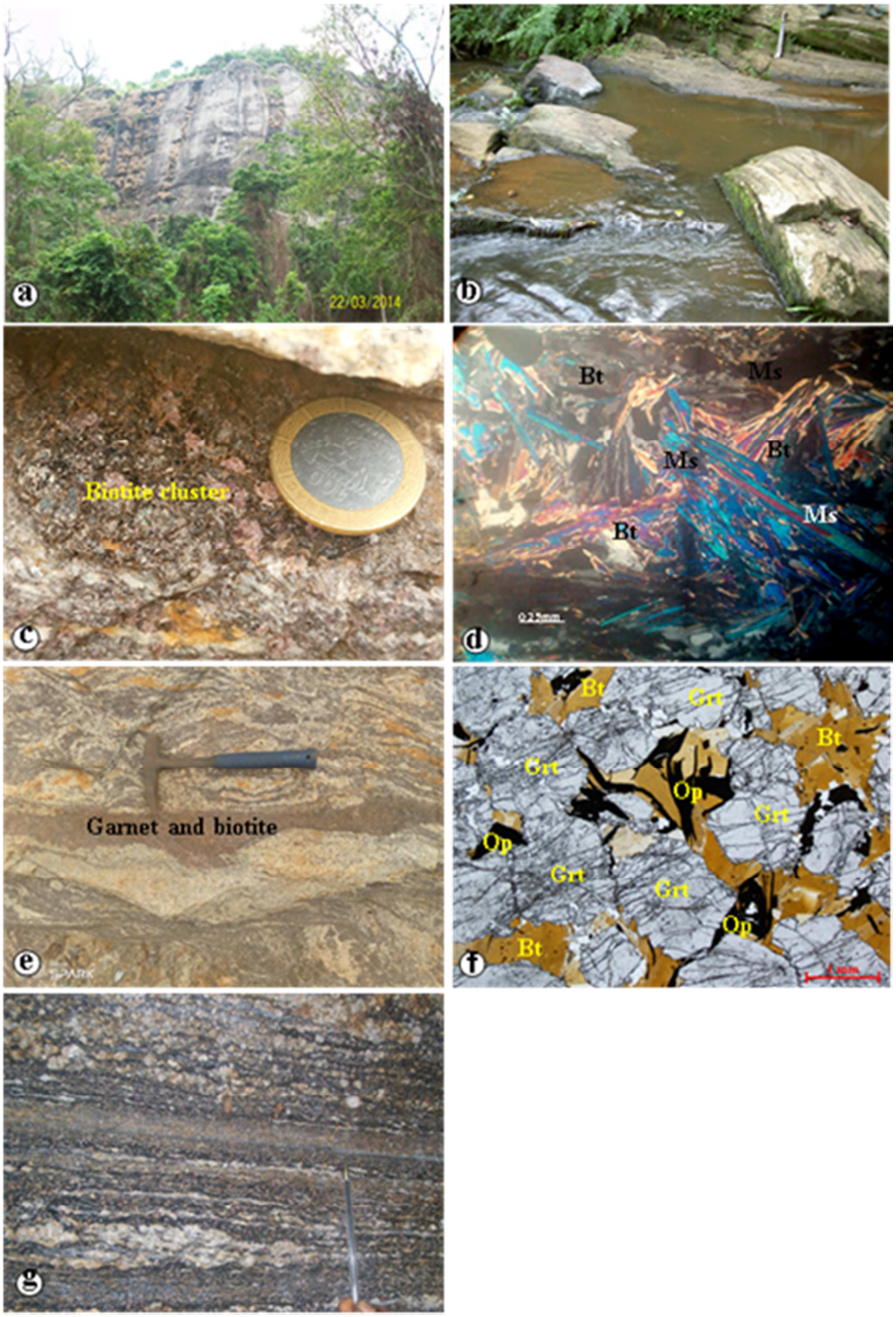

Figure 7. *Photographs and microphotographs of Grt-Ky migmatites: (a) Sigmoidal quartz-feldspar boudins; (b) Oriented kyanite; (c) Traces of partial melting showing migmatization; (d) Heterogranular granolepidonematoblastic texture; (e) Lepidoblastic layers alternating with granoblastic layers; (f, g) Retromorphosis of plagioclase and kyanite to muscovite; h) Weathering of plagioclase porphyroblast.*

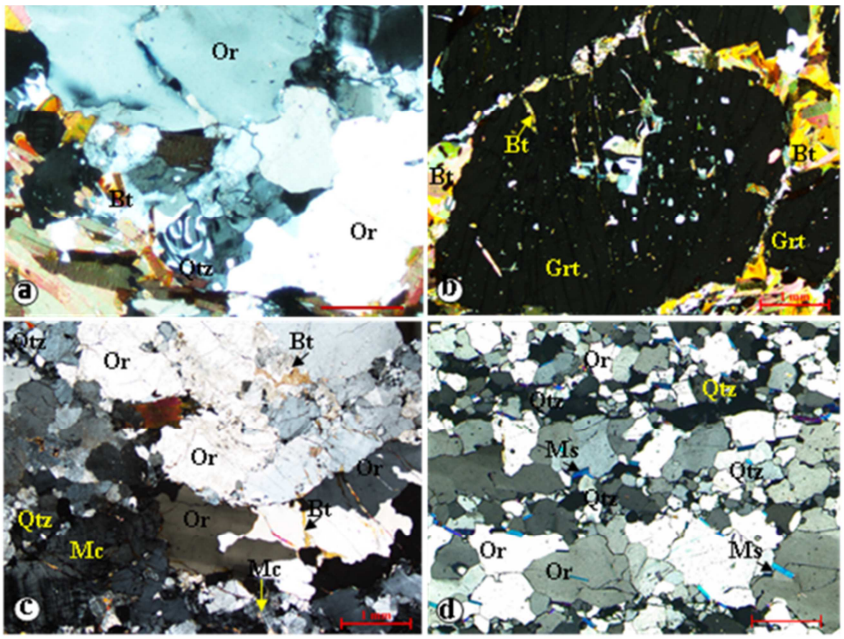

Figure 8. *Microphotographs of Grt-Ky migmatites showing: (a) Myrmekitic texture; (b) Internal schistosity in garnet porphyroblasts; (c) Microcline patches with quartz inclusion; (d) Leucosome with oriented muscovite lamellae.*

5. Whole-Rock Geochemistry

5.1. Major Element Compositions

The chemical composition in major elements (Table 1) varies from one petrographic type to another. The lowest SiO_2, P_2O_5 and K_2O contents are 42.66, 0.04 and 1.13% respectively in Grt-ky migmatites, whereas the highest contents are 75.4, 0.41 and 4.42 respectively in Grt-Chl schists. The lowest Al_2O_3, Fe_2O_3, CaO, MgO, TiO_2, MnO and Cr_2O_5 contents are 9.97%, 4.9%, 0.17%, 1.21%, 0.57%, 0.09% and 0.009 % respectively in Grt-Chl schists while the highest contents are 19.92%, 23.23%, 7.13%, 7.46%, 3.46%, 1.88% and 0.58% respectively in Grt-ky migmatites. The lowest Na_2O (0.6 %) and the highest Cr_2O_3 (0.13%) contents are in Grt micaschists. A/CNK ratio (1.28-4.74) reflects the hyperaluminous feature of rocks, typical of clayey sedimentary rocks. The sum (Fe_2O_3 + MgO + TiO_2) varies widely from 7.3 to 32.6%, enlightening various lithological units. Na_2O (0.6-3.08%) and K_2O (1.13-4.42%) contents suggest a variable detrital feldspathic load in sedimentary sequences that preceded the metamorphism. K_2O/Na_2O ratios vary from 0.44 to 4.43, according to Taylor and McLennan [72]; this ratio is < 1 in shales and > 1 in greywackes. CaO (0.17-7.13%) and TiO_2 (0.57-1.88%) contents are also variable, reflecting the richness or poverty of plagioclase (anorthite) and titanium minerals respectively. TiO_2/Al_2O_3 ratios (0.05-0.1) are slightly higher than in clays (0.04, [24]) and within the range of Yaoundé, Dibang and Boumnyebel metasediments (0.05-0.075; [52, 99, 81], and continental or nearshore clay and arenaceous sediments [39]. Low grade minerals (chlorite) and high grade minerals (kyanite) in rocks indicate low to high grade metamorphism. The variation of this metamorphic gradient leads to a redistribution of some oxides such as K_2O and Na_2O while TiO_2 is immobile. In the TiO_2 versus SiO_2 diagram of [70], the investigated samples plot in the field of sedimentary rocks (Figure 9). Similar protolith was proposed by Nzenti et al., Stendal et al. and Yonta-Ngoune [52, 69, 81].

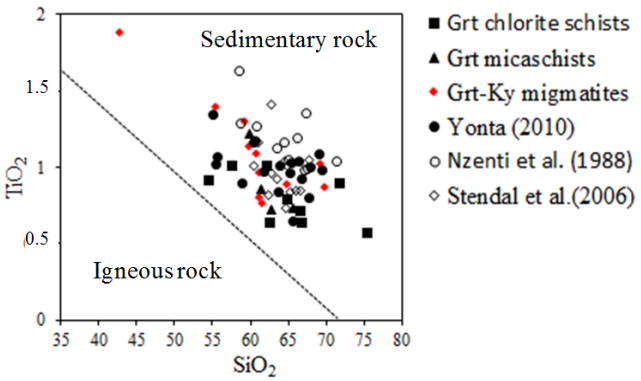

Figure 9. *TiO_2 vs SiO_2 diagram of [70] indicating the protolith of rocks studied.*

Table 1. *Rock sample geochemistry of major and trace elements.*

Type	Grt chl schists									Grt micaschists			
Sample (%)	**C4E1**	**C3E10**	**KS01**	**KS02**	**KS04**	**KB01**	**KB02**	**MB 12**	**MB 13**	**C4E24**	**C1E7**	**C1E10**	**MB03**
SiO_2	62.4	75.4	54.5	66.71	66.47	64.71	71.7	57.41	62.14	65.6	59.9	61.4	62.74
Al_2O_3	11.75	9.97	18.8	11.32	12.57	13.65	12.84	18.36	17.09	11.6	16.4	14.1	14.59
Fe_2O_3	5.95	6.4	9.24	4.9	5.18	6.68	6.92	9.49	8.84	12.7	11.9	14.35	6.62
CaO	4.99	1.52	1.52	4.63	3.4	2.94	1.16	0.17	1.46	1.37	1.42	2.55	4.26

Type	Grt chl schists									Grt micaschists			
Sample (%)	**C4E1**	**C3E10**	**KS01**	**KS02**	**KS04**	**KB01**	**KB02**	**MB 12**	**MB 13**	**C4E24**	**C1E7**	**C1E10**	**MB03**
MgO	1.91	1.6	3.71	1.8	1.8	2.5	1.21	4.28	3.17	2.34	3.36	3.3	2.68
Na_2O	1.66	1.71	1.48	1.22	2.58	2.04	0.65	1.68	1.61	0.6	0.67	1.18	2.96
K_2O	2.49	1.55	4.42	2.72	2.31	2.53	2.17	2.98	2.82	2.14	2.97	1.82	3.16
Cr_2O_3	0.04	0.07	0.02	0.009	0.01	0.012	0.01	0.018	0.019	0.13	0.1	0.09	0.012
TiO_2	0.64	0.57	0.92	0.64	0.72	0.79	0.9	1.01	1.01	0.73	1.22	0.86	0.72
MnO	0.13	0.11	0.09	0.11	0.09	0.12	0.13	0.1	0.22	0.41	0.22	0.29	0.1
P_2O_5	0.16	0.41	0.18	0.12	0.15	0.16	0.05	0.16	0.16	0.11	0.19	0.24	0.13
LOI	7.51	0.49	4.8	5.6	4.5	3.6	2.1	4	1.2	0.79	0.71	-0.04	1.8
Total	99.63	99.8	100	99.9	99.86	99.8	99.9	95.66	98.54	98.5	99.06	100	99.8
A/CNK	1.286	2.086	2.53	1.32	1.5163	1.818	3.23	3.8	2.902	2.822	3.24	2.541	1.41
K_2O/Na_2O	1.5	0.906	2.99	2.23	0.8953	1.24	3.34	1.77	1.752	3.567	4.43	1.542	1.07
TiO_2/Al_2O_3	0.054	0.057	0.05	0.06	0.0573	0.058	0.07	0.06	0.059	0.063	0.07	0.061	0.05
Sample (ppm)	C4E1	C3E10	KS01	KS02	KS04	KB01	KB02	MB12	MB13	C4E24	C1E7	C1E10	MB03
Ba	400	284	768	502	395	621	457	1256	617	537	605	325	741
Ni	36	64	65	31	30	41	<20	70	103	46	75	49	37
Sc	10	10	21	11	11	14	14	22	22	19	23	30	16
Co	15	16	22.3	11.9	11.7	18.4	15.8	19	43.2	18	27	24	19.7
Cs	6.33	2.64	11	6.7	6.8	6	2.1	2.8	5.2	3.57	4.3	5.5	0.8
Ga	19.9	15.1	25.9	15.6	14.8	17	15.8	23.6	20.7	17.3	22	15	19.4
Hf	4.2	3.1	5.6	6	7.4	5.8	10.4	5.5	5.7	5.3	6.4	5.3	5.2
Nb	10.8	6.4	16.4	11.3	11.8	13	13.4	15.1	13.2	11.2	16	14	13.1
Rb	103.5	58.5	188	116	103	105	90.2	111	114	70.5	109	91	95.8
Sn	3	1	4	3	3	3	2	3	2	2	3	2	1
Sr	213	111.5	124	244	188	186	82.4	84.3	123	37	61	56	281
Ta	0.6	0.5	1	0.7	0.9	1	1	1	0.8	0.9	1.2	1.1	0.7
Th	8.8	4.57	13.8	10.1	12.7	10.4	10.8	12.6	11.3	7.43	9.9	9.9	9.5
U	1.2	1.48	3.3	2.2	2.4	2.4	2.6	2	2.4	1.19	1.7	3	1.3
V	90	100	167	89	87	119	88	178	191	99	186	134	114
W	1	1	2.6	1.6	1.6	1.6	1.3	2.1	1.5	1	1	2	<0.5
Zr	149	101	200	209	270	215	379.2	205	211	203	216	195	207
Y	25.9	23.4	38.5	27.1	28	31.2	27.2	6.2	36.2	33.3	37	63	21.8
La	25.6	19.5	44.3	32.5	39.5	36.5	48.8	3	39.7	14.1	29	12	48.6
Ce	54.1	43.7	85.1	65.1	78.1	72.8	82.7	4.3	80.5	30.8	71	70	87.2
Pr	6.43	5.57	10	7.18	8.4	8.21	10.67	0.56	9.07	4.13	7.2	3.7	8.76
Nd	24.6	25.6	36.8	27.1	31.1	31.4	39.5	2.2	35.5	14.9	29	16	29.8
Sm	5	6.43	7.46	5.37	6.01	6.45	7.35	0.44	7.1	3.21	6.2	4.8	5.09
Eu	1	1.42	1.55	1.07	1.28	1.4	1.58	0.1	1.59	0.84	1.5	1.4	1.38
Gd	4.81	6.02	7.16	4.96	5.85	5.98	6.77	0.56	6.88	4.95	6.1	7.4	4.64
Tb	0.71	0.91	1.11	0.83	0.88	0.89	0.98	0.12	1.05	0.9	1.1	1.6	0.69
Dy	4.8	5.05	6.76	4.83	5.09	5.53	5.39	1.01	6.71	6.04	7	12	3.88
Ho	0.95	0.84	1.41	1	1.04	1.08	1.02	0.23	1.41	1.28	1.4	2.3	0.76
Er	2.77	2.42	3.96	2.97	3.05	3.2	3.1	0.95	4.02	3.43	4.4	6.7	2.27
Tm	0.43	0.38	0.53	0.46	0.45	0.46	0.47	0.17	0.58	0.57	0.6	1.1	0.32
Yb	2.95	3.08	3.36	3.02	2.79	3.03	3.22	1.33	4.12	3.67	3.4	7	2.22
Lu	0.48	0.43	0.48	0.46	0.43	0.47	0.53	0.25	0.61	0.58	0.6	1	0.31
La_N/Yb_N	5.895	4.301	8.96	7.31	9.6177	8.183	10.3	1.53	6.546	2.61	5.82	1.203	14.9
La_N/Sm_N	3.197	1.894	3.71	3.78	4.1043	3.534	4.15	4.26	3.492	2.743	2.91	1.61	5.96
Eu/Eu*	0.622	0.696	0.65	0.63	0.658	0.687	0.68	0.61	0.693	0.642	0.75	0.697	0.87
Gd_N/Yp_N	1.319	1.581	1.72	1.33	1.6964	1.597	1.7	0.34	1.351	1.091	1.48	0.851	1.69
Th/U	7.333	3.088	4.18	4.59	5.29	4.33	4.15	6.3	4.71	6.24	5.8	3.3	7.31

Type	Grt-Ky migmatites										
Sample (%)	**C4E12**	**C1E14**	**C2E19**	**C2E6**	**AN1**	**AN3**	**NE1**	**NE2**	**AN2**	**EL3**	**AN4B**
SiO_2	55.4	69.7	64.7	60.7	61.2	61.22	69.14	59.15	61.44	59.86	42.66
Al_2O_3	17.4	13.4	14	15.9	17.35	16.2	12.26	17.35	15.67	16.02	19.92
Fe_2O_3	8.67	8.22	8.6	10.65	8.52	6.9	8.12	10.89	6.47	8.28	23.23
CaO	7.13	1.3	2.48	2.15	3.09	4.4	2.01	1.31	4.98	4.83	2.4
MgO	3.11	2	1.84	2.7	2.84	4.09	2.68	3.78	4.34	4.44	7.46
Na_2O	3.46	1.49	3.08	1.91	2.87	2.3	1.55	1.29	2.11	1.98	0.67
K_2O	1.53	2.55	2.03	2.13	1.86	2.05	2.49	3.8	2.05	2.07	1.13
Cr_2O_3	0.05	0.09	0.11	0.12	0.016	0.02	0.017	0.023	0.021	0.021	0.047
TiO_2	1.4	0.87	0.89	1.09	0.97	0.8	1.02	1.3	0.77	1.14	1.88
MnO	0.12	0.17	0.13	0.22	0.26	0.12	0.14	0.18	0.1	0.15	0.58
P_2O_5	0.37	0.13	0.16	0.22	0.12	0.22	0.6	0.21	0.23	0.28	0.04
LOI	0.82	0.08	0.56	1.06	0.7	1.3	-0.3	0.4	1.5	0.6	-0.4
Total	99.5	100	98.6	98.9	99.8	99.6	99.7	99.7	99.7	99.7	99.6

Type	Grt-Ky migmatites										
Sample (%)	**C4E12**	**C1E14**	**C2E19**	**C2E6**	**AN1**	**AN3**	**NE1**	**NE2**	**AN2**	**EL3**	**AN4B**
A/CNK	1.44	2.51	1.84	2.57	2.2187	1.85	2.03	2.71	1.71	1.8	4.743
K_2O/Na_2O	0.44	1.71	0.66	1.12	0.6481	0.89	1.61	2.95	0.97	1.05	1.687
TiO_2/Al_2O_3	0.08	0.06	0.06	0.07	0.0559	0.05	0.08	0.07	0.05	0.07	0.094
Sample (ppm)	C4E12	C1E14	C2E19	C2E6	AN1	AN3	NE1	NE2	AN2	EL3	AN4B
Ba	630	938	387	594	395	866	638	976	814	780	278
Ni	15	64	29	88	75	84	56	89	103	51	160
Sc	14	15	14	20	18	12	18	26	11	16	62
Co	20	19	13	27	24.3	21	19	29	21	21.5	62.8
Cs	0.74	1.34	2.2	2.52	1.1	4.4	1.4	1.8	4.3	3.5	1.1
Ga	20.8	17.2	18.9	19.9	19.6	19	14	19	18	21	13.1
Hf	9.8	6.4	6.5	5.7	5.7	5.4	7	6.4	5.8	6.2	8
Nb	13.6	11.9	10.6	13.4	13.5	8.5	15	14	9.3	10	31.3
Rb	63.6	81.5	83.3	76.1	66.8	85	85	127	79	116	49.8
Sn	2	1	1	1	1	1	1	1	2	1	<1
Sr	550	202	273	190	251	529	147	135	543	400	61.3
Ta	0.7	0.9	0.6	0.9	0.9	0.4	1.2	0.8	0.6	0.7	2.3
Th	21.1	10.1	7.03	9.34	11.7	7.6	8.5	14	7.8	8.4	8.2
U	1.64	1.56	0.79	1.78	2.3	1.7	1.9	2.3	1.6	1.7	1.9
V	159	128	109	198	150	114	170	236	110	139	333
W	1	1	<1	1	1.5	2.1	1.3	1.1	2.6	<0.5	2.1
Zr	415	220	221	205	205	208	258	232	212	238	289.3
Y	23.7	30	29	35.5	35.3	21	41	44	16	21.8	111.1
La	94.7	32.1	26.3	18.1	34.6	39	36	44	38	40.7	26.2
Ce	185	64.2	54.9	38.1	68.8	76	83	90	74	85.2	50.4
Pr	21.4	7.88	6.76	4.73	7.88	9	11	11	8.7	10	5.91
Nd	85.5	31	26.9	19.8	30.1	35	47	41	33	38.8	22.5
Sm	13.7	6.5	5.84	4.85	6.07	6.3	12	8.5	5.9	6.95	6.06
Eu	3.04	1.38	1.61	1.16	1.56	1.5	1.5	1.6	1.4	1.53	0.97
Gd	8.42	5.34	5.08	5.47	6.15	5.3	11	8.2	4.5	5.76	12.27
Tb	0.95	0.83	0.89	0.92	1.03	0.7	1.4	1.3	0.6	0.79	2.75
Dy	5.27	5.46	5.36	6.25	6.1	3.7	7.4	7.9	3.2	4.47	19.04
Ho	0.86	1.05	1.07	1.23	1.26	0.7	1.4	1.6	0.6	0.8	4.22
Er	2.74	3.27	3.15	3.63	3.73	2	4.2	4.7	1.7	2.16	12.54
Tm	0.37	0.63	0.4	0.51	0.57	0.3	0.6	0.7	0.2	0.27	1.82
Yb	2.14	3.22	3.09	3.63	3.57	2	4	4.7	1.5	1.84	11.73
Lu	0.36	0.47	0.49	0.54	0.56	0.3	0.6	0.7	0.2	0.25	1.86
La_N/Yb_N	30.1	6.77	5.78	3.39	6.5839	13.6	6.05	6.38	17.4	15	1.517
La_N/Sm_N	4.33	3.08	2.81	2.33	3.5596	3.88	1.87	3.27	4.04	3.66	2.7
Eu/Eu*	0.86	0.71	0.9	0.69	0.7783	0.78	0.4	0.59	0.82	0.74	0.343
Gd_N/Yp_N	3.18	1.34	1.33	1.22	1.3937	2.16	2.23	1.4	2.47	2.53	0.846
Th/U	12.9	6.44	8.9	5.25	5.09	4.5	4.5	6.2	4.9	0.94	0.94

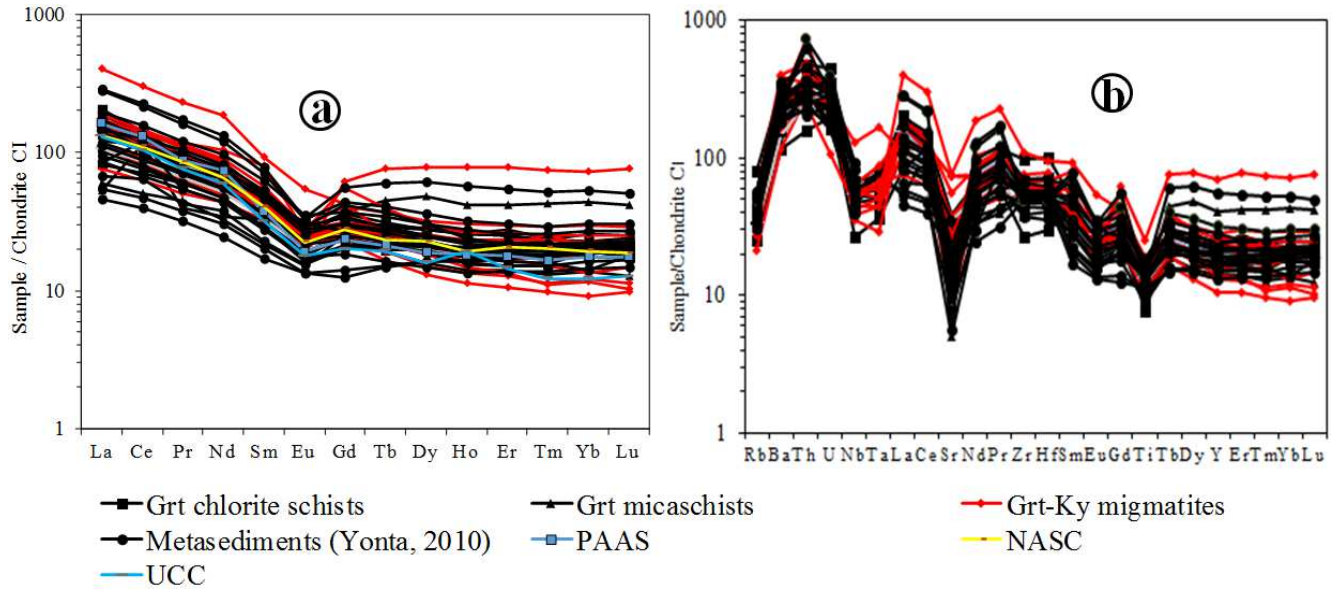

Figure 10. *a) RE spectrum; (a) and multi-element spectra; (b) of rocks compared with those of Boumnyebel [81]. Normalisation with the values of [36].*

5.2. Trace Elements Including REEs

Rare earth elements (REE) patterns (Figure 10a) are fairly homogeneous and fractionated ($1.20 \leq La_N/Yb_N \leq 17.35$) with negative Eu anomalies ($0.34 \leq Eu/Eu^* \leq 0.90$). In terms of the total REE contents (∑REE), the metasediments of the Yaoundé group range from 15.22 to 423.9 ppm (avg. ∑REE = 174.98 ppm) showing coherent chondrite-normalized REE patterns. The average $(La/Yb)_N$ and $(La/Lu)_N$ ratio, 8.31 and 8.30 respectively, do not show highly fractionated REE patterns. The spectra (Figure 10) are similar to UCC (Upper Continental Crust) [67], PAAS (Post-Archean Australian Shale) [72], and NASC (North American shale composite) [27]. These spectra characterize continental origin materials with an enrichment of light rare earths (LREE; $1.60 \leq La_N/Sm_N \leq 5.96$) compared to heavy rare earths (HREE; $0.34 \leq Gd_N/Yb_N \leq 2.53$) with low fractionation and flat spectra. The multi-element diagram (Figure 10b) shows regular spectra with pronounced negative Sr, Nb Ta and Ti anomalies. The spectra are flat from Tb to Lu. The average values of Ni (63.52), V/Ni (2.76) and Ni/Co (2.81) ratios are similar to those of post-Archean fine-grained sediments [50]. La vs Th diagram of [37] confirms the post-Archean age of the Yaoundé metasediments (Figure 11).

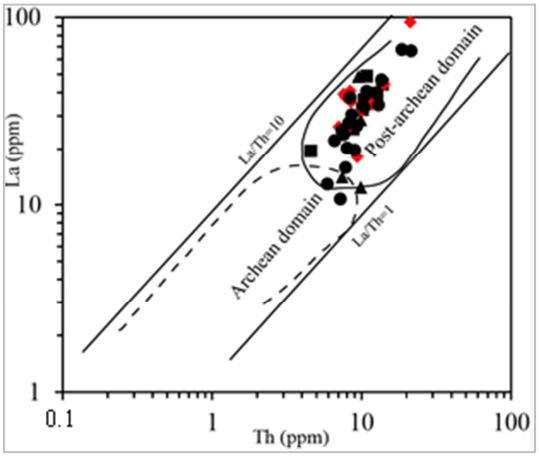

Figure 11. *La vs Th diagram of [37] showing the source of rocks studied.*

6. Discussion

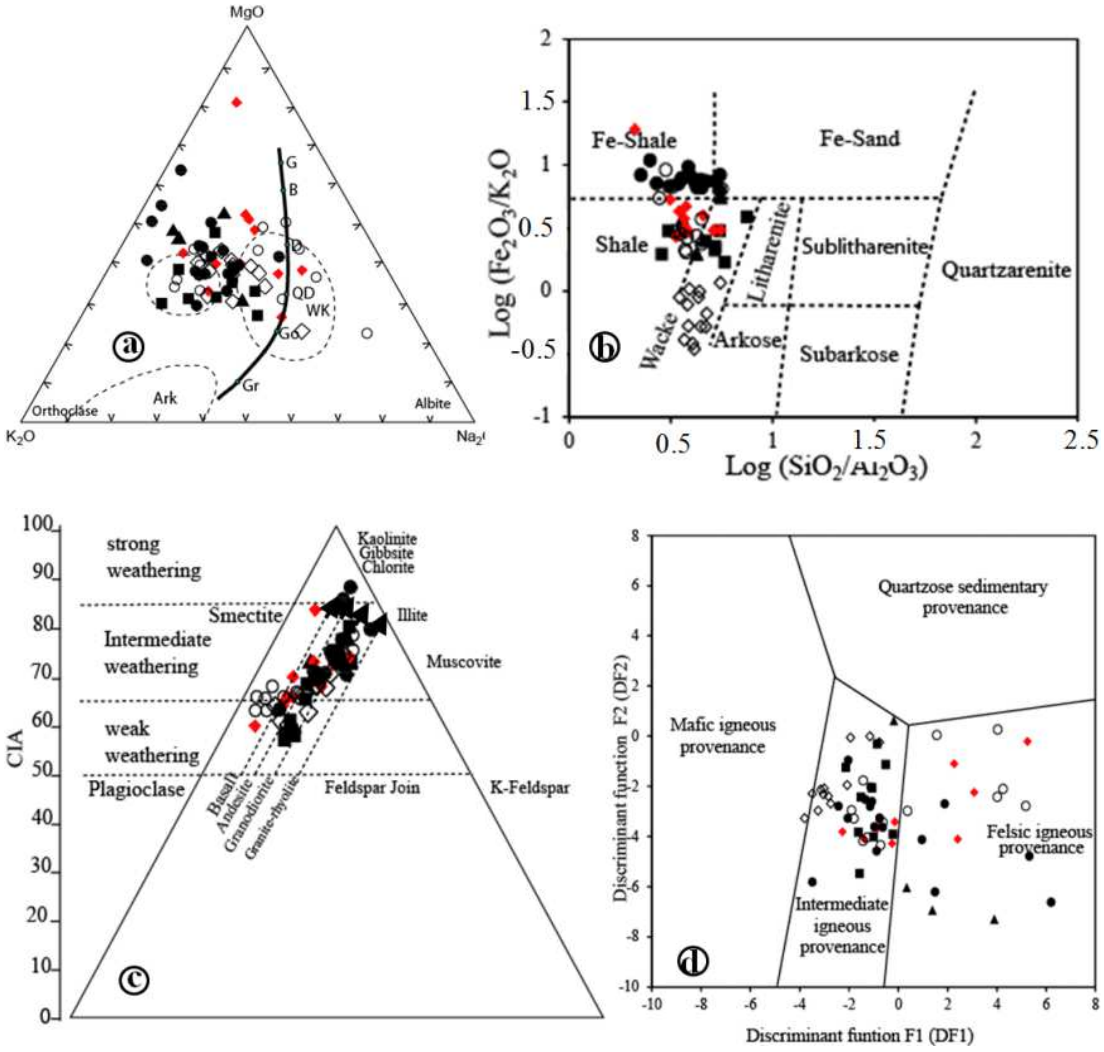

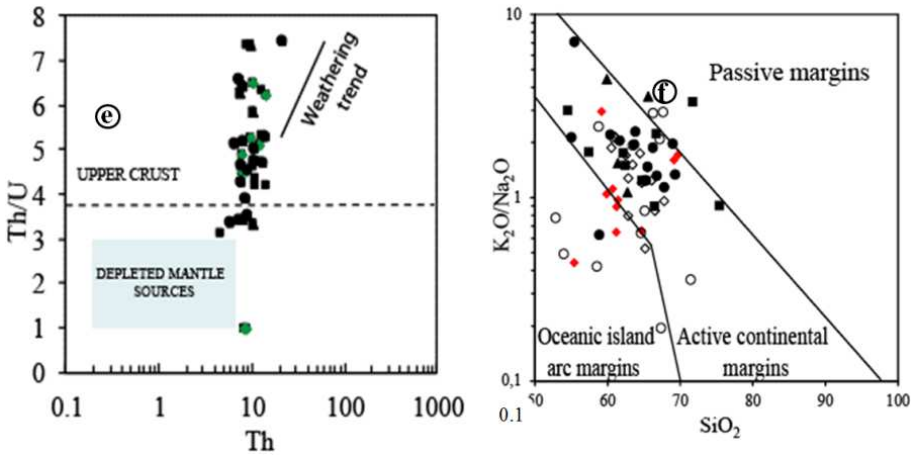

Figure 12. *Geochemical diagram of major and trace elements in rocks studied compared to those of Yaoundé [52], Dibang [69] and Boumnyebel [81]: a) MgO-K_2O-Na_2O [14]; b) Log (Fe_2O_3/K_2O) vs Log (SiO_2/Al_2O_3) of [28]; c) A-CN-K and CIA diagram of [18]; d) Discriminant Function Diagram (after [65]): DF1= -1.773TiO_2 + 0.607Al_2O_3 + 0.76Fe_2O_3 - 1.5MgO + 0.616CaO + 0.509Na_2O - 1.224K_2O-9.09; DF2= 0.445TiO_2 + 0.07Al_2O_3 - 0.25Fe_2O_3 -1.142MgO + 0.438CaO 438CaO + 1.475Na_2O + 1.426K_2O - 6.861; e) Th/U versus U plot for Shimla and Chail meta-sediments [37]; f) K_2O/Na_2O vs SiO_2 diagram (after [66]).*

In the last decades, the continental crust and near-surface environment got much attention in Cameroon and worldwide [72, 50, 34, 5, 30, 20]. The source composition of weathered rocks/sediments, tectonic setting, maturity, provenance, weathering history, and palaeoenvironment of basins were inferred using fine-grained terrigenous sediments [37, 4, 6, 35, 66, 30]. In this paper, the metasediments were studied to decipher the provenance and geodynamic context. Nzenti et al. and Yonta-Ngoune [52, 81] also described the metasediments in other areas. Similar formations are described in the Siguiri [19], NE Brazil [55, 33], SW Nigeria [10] and central India [12] basins. Petrography of metasedimentary rocks shows parageneses with prograde metamorphism from greenschist facies (Grt chlorite schists: Chl + Amph + Qtz + Grt + Bt + Pl + Kfs) to granulite facies (Grt-ky migmatites: Qtz + Ms + Bt + Grt + Pl + Kfs + Amph ± Ky) through amphibolite facies (Grt micaschists: Qtz + Bt + Ms + Pl + Grt + Or + Amph + Ky + Mc). Similar parageneses and facies were observed in SW Nigeria [10], parts of Togo and Ghana West Africa [1], Yaoundé migmatites [52], and in NE Brazil, which is the SW continuity of the Central African Pan-African belt [56].

6.1. Sources of Metasediments

Some major elements are likely to be mobilized during metamorphism and some weathering processes. These elements can thus be used to highlight the sources of the studied metasediments. The MgO-K_2O-Na_2O diagram of [14] and Log (Fe_2O_3/K_2O) versus Log (SiO_2/Al_2O_3) diagram of [28], place the metasediments of the Yaoundé Group in the field of shales and greywackes (Figure 12a and Figure 12b). The [18] diagram shows they originate mainly from andesites and granodiorites with an intermediate chemical alteration index (Figure 12c), intermediate to incidental felsic magmatic source (Figure 12d; [65]).

Average U and Th concentrations in studied metasediments are similar to the values of Yonta Ngoune [81] (Figure 12e). Average Th/U ratios above 4.0 in sedimentary rocks portray intense weathering in source areas or sediment recycling [37]. A wide range of Th/U ratios of the southwestern Yaoundé Group metasediments (1.36-8.81) in the Th/U vs. Th diagram [37]; Figure 12e) shows varying degrees of weathering and recycling; most samples plot toward the weathering trend with progressively higher Th/U values as observed by [30]. The erosion of an old continental crust cannot explain the low to high CaO (0.17-7.13%) and Sr (37-550 ppm) contents, but high values rather suggest the influence of volcanic material [50]. Negative Eu anomalies ($0.34 \leq Eu/Eu^* \leq 0.90$) and La_N/Yb_N ratios (1.20-17.35) indicate low feldspar in the protolith of studied metasediments. High Ba (616.833), V (145.333) and Zr (227.591) values suggest continental source materials. The mean ratios of Nb/Ta (15.25), Zr/Hf (36.52) and Y/Ho (27.41) are close to those of the upper continental crust [72]. The Rb/Cs ratio (38.09) is consistent with the lowest value in the upper continental crust, about 30 [72]. The low content of highly charged elements (Nb, Ti) compared to neighboring incompatible elements, expressed as negative anomalies (Figure 10b), average Th/U values greater than 4 (table 1), relative deficit of alkaline earth elements (Ca, Sr) compared to neighboring incompatible elements (Table 1 and Figure 10b) and the marked fractionation of the element ratios of high Rb/Sr (0.72) and low Sm/Nd (0.21) radioactive pairs compared to estimated values (0.03 and 0.33 respectively), account for the erosion of the UCC source material [72].

6.2. Geodynamic Environment of Deposition

Many classifications highlight the correlation between the chemical composition of detrital sediments and their geodynamic depositional environment. Sedimentary series related to oceanic island arc (OIA) setting show a similar andesitic composition to that of the total crust [17, 71]. Detrital series related to a continental island arc (CIA) display a similar composition to that of the continental crust or continental calc-alkaline rocks [29, 2]. The composition of detrital sedimentary series associated with active continental margins (ACM) is similar to that of the crystalline basement corresponding to the

upper continental crust [71]. Detrital series of passive continental margins (PCM) correspond to very mature sediments with a composition similar to the platform sedimentary covers [64]. Thus, the diagram of [66] places the studied rocks mainly in the active continental margin (Figure 12f) despite few samples in the oceanic island arc domain, also confirmed by the diagram of [7] (Figure 13a). Data from [52, 69, 81] also plot in the active continental margin (Figure 12f and Figure 13a). The hypothesis of active margin and/or oceanic island arc using geochemical data is supported by Toteu at al. [78] who suggest from geochronological data a northward subduction context. The Yaoundé basin results from extensional processes in the northern Congo craton, which guided rifting, fragmentation and limited oceanization [50]. Furthermore, the ophiolitic affinity of rocks of the Yaoundé Group reinforces this hypothesis [51, 41]. In the same context, [20] from petrological and isotopic (Ar-Ar) studies situate the Mamb calk-alkaline pluton in an oceanic island arc context that extends eastward to Yaoundé and up to Lomié in the SE Cameroon. They proposed a south-north subduction of the Pan-African Yaoundé hot oceanic crust under the Archean Adamawa-Yade block.

TiO_2 vs FeO*/MgO diagram of [40] also shows a tholeiitic affinity (Figure 13b). Tholeiites characterize rocks of distension zones, evidence of the probable ocean. REE contents of the studied metasediments is almost identical to that of the PAAS, with a flat spectrum (Figure 13c) and average REE/PAAS ratios close to 1 (0.86-1.31). Samples from [52, 69, 81] and this study similarly plot in the same field in tectonic discrimination diagrams, showing homogeneous and sub-parallel REE and multi-element spectra (Figures 10a, 10b) suggesting a similar geodynamic and depositional environment. Precambrian sediments indicate fairly high alteration indices [44, 13, 18, 63]. These results partially tie with this study and those of Nzenti et al., Stendal et al. and Yonta-Ngoune [52, 69, 81] with the chemical weathering index incidentally low to high and mostly intermediate (Figure 8c). The source rocks of the Yaoundé Group metasediments are predominantly granodiorites and andesites (Figure 12c). Owona et al. [58] indicate the emplacement of the source deposits of the Yaoundé Group after the Eburnian orogeny during a prolonged erosion phase of the Congo craton margin in the Central Africa. Granodiorites and andesites, sources of the southwestern metasediments of the Yaoundé Group, are likely to be related to the formations of the Congo craton. Oliveira et al. [54] demonstrated with Sm-Nd isotope geochemistry and U-Pb age dating that most clastic metasedimentary rocks in both belts of Yaoundé and Sergipano derived from the northern sources and, to a lesser degree, from cratons in the south. The northern source is probably the Archean Adamawa-Yade block, considered a microcontinent separated from the northern edge of the Congo craton [50, 74, 20, 41]. Mukete et al. [41] show that the compositions of spinel and ultramafic whole rocks reveal an arc setting that evolved from divergent to convergent plate setting. The results of aforementioned works and of this study show that the metasedimentary rocks from the southwestern portion of the Yaoundé Group derive mainly from the intermediate weathering of rocks of the Congo craton and or the Adamawa-Yade block.

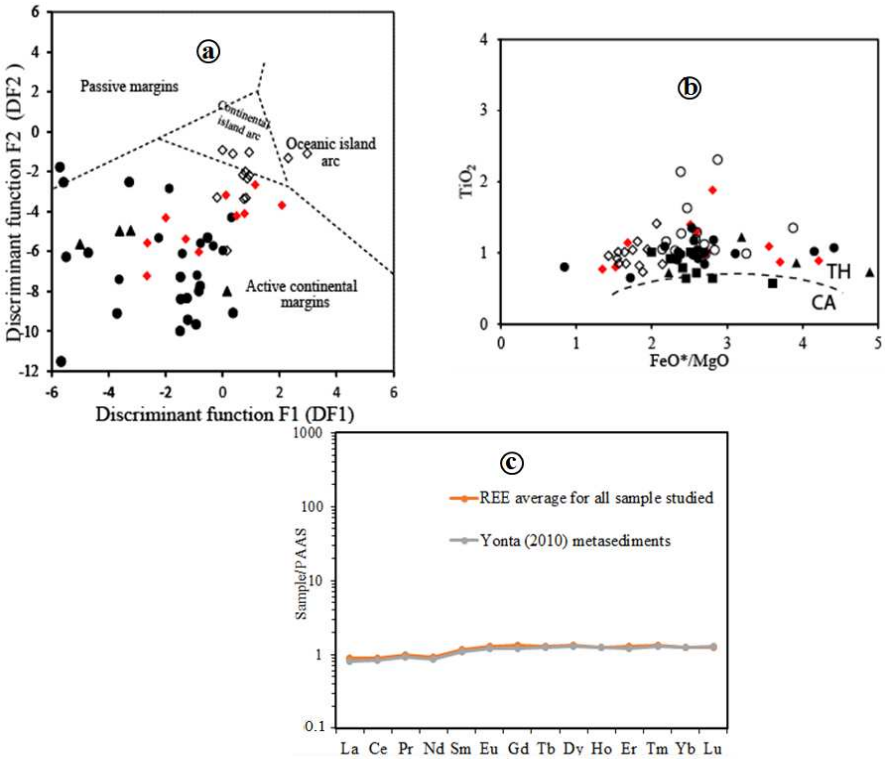

Figure 13. *a) Discriminant Function Diagram (after [6]; DF1 refer to - 0.447SiO_2 + 0.972TiO_2 + 0.008Al_2O_3 - 0.267Fe_2O_3 + 0.208FeO - 3.082MnO + 0.14MgO + 1.95CaO + 0.719Na_2O + 0.032K_2O + 7.51P_2O_5 + 0.303 and DF2- 0.421SiO_2 + 1.988TiO_2 - 0.526Al_2O_3-0.551Fe_2O_3 - 1.61FeO + 2.72MnO + 0.881MgO - 0.907CaO - 0.177Na_2O - 1.84K_2O + 7.244P_2O_5 + 43.57, respectively. Ark: arkose; Sh: shale; GW: greywacke; Gr: granite; Gd: granodiorite; Do: Diorite; Ga: gabbro; b) TiO_2 vs FeO*/MgO diagram of Miyashiro (1974); c) Spectrum of average RRE values vs PAAS values.*

6.3. Correlation Between the Neoproterozoic Sergipano Belt (NE Brazil) and the Yaoundé Belt (Cameroon, Africa)

Oliveira et al. [54] carried out pioneer works on the correlation between the Sergipano belt and the Yaoundé Belt. They described contemporaneous metasedimentary rocks in both belts: the Yaoundé belt comprises schists, quartzites, gneisses and migmatitic gneisses all involved in a collision estimated between 620 and 610 Ma, the Sergipano belt which includes in addition to metasedimentary rocks, migmatitic gneisses and two metavolcano-plutonic complexes involved in a collision at 618 ± 12 Ma. [57] testify in the Sergipano belt a syn- to late-collisional sedimentary influx toward the São Francisco craton (SFC) in the south. This supports the work of [16] who suggests the sediments at the origin of the Sergipano belt derive from the erosion of the SFC. In Cameroon, the works of [50] and the present paper show that the sediments at the origin of the Yaoundé Group probably derive from the erosion of the Congo craton, which is the eastern continuity of the SFC [54]. In the Sergipano belt, the sediments of the Macuréré domain are mainly from the Borborema Province in the north. This is consistent with the erosional sediments in the Adamawa-Yadé Archean block north of the Yaoundé Group as highlighted by [50, 74, 20]. The Sergipano belt is located between the Sao Francisco craton in the south and the Borborema Province [57]. This arrangement suggests that the Archean block of Adamawa Yadé is the plunge of the Borborema Province in Central Africa. [32] suggest that the sediments of the Araticum paleobasin (Sergipano fold belt) were deposited in an oceanic environment during the exhumation of arcs in the Brasilian-Pan-African orogeny. This supports the hypothesis of [50] and of this study, which suggest the sediments at the origin of the Yaoundé Group were deposited in a probably oceanic environment. The hypothesis of oceanization is also supported by D'el-Rey Silva [15], through intensive geological mapping (scales 1:50 000 and 1: 100,000), in a key area of the southern part of the Sergipano belt; his similar stratigraphic and structural data explain the tectonic evolution of the belt in terms of the closure of an asymmetric, laterally continuous basin infilled under a syn-depositional extension regime and evolving into an oceanic basin (the Canindé Sea). Structural analysis in both areas (Yaoundé and Sergipano belts) shows that the second phase of deformation is associated with thrusting Neoproterozoic supracrustal rocks toward the Congo craton [52, 53] and the SFC [33] respectively. Most Sergipano belt and the Yaoundé Group features are similar. This correlation suggests, a model compatible with the supercontinent that evolved by fragmentation and amalgamation along lived zones of lithosphere weakness throughout the Proterozoic [15].

7. Conclusion

The metasediment rocks of the Yaoundé Group comprise Grt chlorite schists, Grt micaschists and Grt-Ky migmatites, dispaying granoblastic to granolepidonematoblastic texture and mineral assemblages of green schist, amphibolite and granulite facies, suggesting prograde metamorphism. The geochemical data reveal wide range of Fe_2O_3 + MgO + TiO_2 contents, from 7.3 to 32.6%, probably reflecting to diversity of lithological units. The protoliths of these metasediments are post-Archean shales and greywackes deriving mostly from the Congo craton and/or the Adamawa-Yadé andesites and granodiorites. The eroded materials are from the upper continental crust source, and were emplaced in an active margin context and/or oceanic island arc.

Declaration of Competing Interest

All the authors do not have any possible conflicts of interest.

Acknowledgements

The authors of this work wish to thank Professor Charles Nkoumbou (Department of Earth Sciences, University of Yaoundé I) for fruitful and constructive scientific exchanges throughout the writing process. The constructive comments by anonymous reviewers are gratefully acknowledged.

References

[1] Attoh, K., Dalmayer, R. D., Affaton, P., 1997. Chronology of nappe assembly in the Pan African Dahomeyide Orogen, West Africa: Evidence from $^{40}Ar/^{39}Ar$ mineral ages. Precambrian Research 82, 153-171.

[2] Bailey, J. C., 1981. Geochemical criteria for a refined tectonic discrimination of orogenic andesites. Chemical Geology 32, 139-154.

[3] Barbey, P., Macaudiere, J., Nzenti, J. P., 1990. High pressure dehydration melting of metapelites: evidence from the migmatites of Yaoundé (Cameroon). Journal of Petrology 31, 401-427.

[4] Basu, H., Dandele, P. S., Kumar, K. R., Achar, K. K., Umamaheswar, K., 2017. Geochemistry of black shales from the Mesoproterozoic Srisailam Formation, Cuddapah basin, India: Implications for provenance, palaeoweathering, tectonics, and timing of Col umbia breakup. Geochemistry 77, 596-61.

[5] Betsi, B. T., Ngo, B. B. L. M., Mvondo, H., Nga, M. Y. L. N., Molotouala, A. C., McFarlane, C., 2020. Rutile LA-ICP-MS U-Pb geochronology and implications for tectono-metamorphic evolution in the Yaoundé Group of the Neoproterozoic Central African Orogeny. Journal of African Earth Sciences 171, 103939.

[6] Bhatia, M. R., Crook, K. A. W. W., 1986. Trace element characteristics of graywackes and tectonic setting discrimination of sedimentary basins. Contributions to Mineralogy and Petrology 92, 181-193.

[7] Bhatia, M. R., 1983. Plate tectonics and geochemical composition of sandstones. J Geol 91, 611-627.

[8] Bouyo Houketchang, M., Penaye, J., Barbey, P., Toteu, S. F., Wandji, P., 2013. Petrology of high-pressure granulite facies metapelites and metabasites from Tcholliré and Banyo regions: Geodynamic implication for the Central African Fold Belt (CAFB) of north- central Cameroon. Precambrian Research 224, 412-433.

[9] Bouyo Houketchang, M., Zhaa, Penaye, J., Zhang, S. H., Njel, U. O., 2015. Neoproterozoic subduction-related metavolcanic and metasedimentary rocks from the Rey Bouba Greenstone Belt of north-central Cameroon in the central African Fold Belt: New insights into a continental arc geodynamic setting. Precambrian research 261, 40-53.

[10] Caby, R., Boessé, J. M., 2001. Pan-African nappe system in southwest Nigeria: the Ife-IIesha schist belt. Journal of African Earth Sciences 33, 211-225.

[11] Champetier de Ribes, G., Aubague, M., 1956. Geological reconnaissance map at 1:500,000, explanatory note on the Yaounde East sheet. Direction of Mining and Geology, Yaounde, Cameroun. Rebon Printing company, Paris, France.

[12] Chattopadhyay, A., Huin, A. K., Khan, A. S., 2002. Structural Framework of Deolapar Area, Central India and its Implications for Proterozoic Nappe Tectonics. Gondwana Research 6, 107-117.

[13] Condie, K. C., 1993. Chemical composition and evolution of the upper continental crust: Contrasting results from surface samples and shales. Chemical Geology 104, 1-37.

[14] De la Roche, H., 1965. On the existence of several geochemical facies in the Palaeozoic shales of the Luchonian Pyrenees. Geologische Rundschau 55, 274-301.

[15] D'el-Rey Silva, L. J. H, 1995. Tectonic evolution of the Sergipano Belt, NE Brazil. Revisia Brasileira de Geociencias 25, 345-332.

[16] D'el-Rey Silva, L. J. H, 1999. Basin infilling in the southern-central part of the Sergipano Belt (NE Brazil) and implications for the evolution of Pan-African/Brasiliano cratons and Neoproterozoic sedimentary cover. Journal South American Earth Sciences 12, 453-470.

[17] Ewart, A., 1976. Mineralogy and chemistry of modern orogenic lavas. Some statistics and implications. Earth and Planetary Sciences Letters, 31, pp. 417-432.

[18] Fedo, C. M., Nesbitt, H. W., Young, G. M., 1995. Unraveling the effects of potassium metasomatism in the sedimentary rocks and paleosols with implications for paleoweathering conditions and provenance. Geology 23, 921-924.

[19] Feybesse, J. L., Billa, M., Diaby, S., Diallo, S., Egal, E., Le Metour, J., Lescuyer, J. L., Sylla, B. I., Villeneuve, M., 2004. Explanatory note of the Geological and Gitological Map at 1/500 000 of Guinea BRGM, DNRGH 60 p. Conakry (GIN).

[20] Fuh, C. G., Nkoumbou, C., Tchakounte Numbem, J., Mukete, K. O., Tchouankoue, J. P., 2021. Petrology, geochemistry, Ar-Ar isotopes of an arc related calk-alkaline pluton from Mamb (Pan-African Yaoundé Group, Cameroon): A testimony to the subduction of a hot oceanic crust. Lithos 384-385, 105973.

[21] Ganwa, A. A., Frisch, W., Siebel, W., Ekodeck, G. E., Cosmas, S. K., Ngako, V., 2008. Archean inheritances in the pyroxene-amphibole-bearing gneiss of the Méiganga area (Central North Cameroon): Geochemical and $^{207}Pb/^{206}Pb$ age imprints. Comptes Rendus Géoscience 340, 211-222.

[22] Ganwa, A. A., Klötzli, U. S., Christoph, H., 2016. Evidence for Archean inheritance in the pre-panafrican crust of central Cameroun: Insight from Zircon Internal Structure and La-Mc ICP-MS U/Pb ages. Journal of African Earth Sciences 120, 12-22.

[23] Ganwa, A. A., Klötzli, U. S., Kepnamou Diguim, A., Hauzenberger, C., 2018. Multiple Ediacaran tectono-metamorphic events in the Adamawa-Yade Domain of the Central Africa Fold Belt: Insight from the zircon U-Pb LAM-ICP-MS geochronology of the metadiorite of Meiganga (Central Cameroon). Geological Journal 53, 2955-2968.

[24] Goldschimdt, V. M., 1954. Geochemistry. Clarendon Press, Oxford.

[25] Goussi Ngalamo, J. F. G., Bisso, D., Abdelsalam, M. G., Atekwana, E. A., Katumwehe, A. B., Ekodeck, G. E., 2017. Geophysical imaging of metacratonizaton in the northern edge of the Congo craton in Cameroon. Journal of African Earth Sciences 129, 94-107.

[26] Goussi Ngalamo, J. F. G., Sobh, M., Bisso, D., Abdelsalam, M. G., Atekwana, E., Ekodeck G. E., 2018. Lithospheric structure beneath the Central African Orogenic Belt in Cameroon from the analysis of satellite gravity and passive seismic data. Tectonophysics 745, 326-337.

[27] Gromet, L. P., Haskin, L. A., Korotev, R. L., Dymek, R. F., 1984. The "North American shale composite": Its compilation, major and trace element characteristics. Geochimica et Cosmochimica Acta 48, 2469-2482.

[28] Herron, M. M., 1988. Geochemical classification of terrigenous sands and shales from core or log data. Journal of Sedimentary Petrology 58, 820-892.

[29] Johnson, R. W., Mackenzie, D. E., Smith, I. E. M., 1978. Volcanic rock associations at convergent plate boundaries: reappraisal of the concept using case histories from Papua-New Guinea. Geol. Soc. America Bull 89, pp. 96-106.

[30] Joshi, K. B., Ray, S., Ahmad, T., Manavalan, S., Aradhi, K. K., 2021. Geochemistry of meta-sediments from Neoproterozoic Shimla and Chail Groups of Outer Lesser Himalaya: Implications for provenance, tectonic setting, and paleo-weathering conditions. Geological Journal 56, 4451-4478.

[31] Kwékam, M., Talla, V., Fozing, E. M., Kouémo, T. J., Dunkl, I.; Njonfang E., 2020. The Pan-African High-K I-Type Granites from Batié Complex, West Cameroon: Age, Origin, and Tectonic Implications. Frontiers in Earth Sciences 8, 383.

[32] Lima, H. M., Pimentel, M. M., Fuck, R. A., Santos, L. C. M. L., Dantas, E. L., 2018. Geochemical and detrital zircon geochronological investigation of the metavolcanosedimentary Araticum complex, Sergipano fold belt: Implications for the evolution of the Borborema Province, NE Brazil. Journal of South American Earth Sciences 86, 176-192.

[33] Lima, H. M., Santos, L. C. M. L., Argollo, R. M., Santos, E. J., 2020. Geological and structural markers of the eastern Borborema Province based on a geotransect covering the Paraíba, Pernambuco, Alagoas and Sergipe states, northeastern Brazil. Journal of the Geological Survey of Brazil 3, 85-95.

[34] Lima, M. M. C., Silva, T. R., Ferreira, V. P., Silva, J. M. R., 2014. Metasedimentary rocks of the northern portion of the Macururé domain, Sergipano Belt, northeastern Brazil: geochemical characterization of their protoliths and tectonic implications. Estudos Geológicos 24, 89-107.

[35] Liu, J., Zhu, Z., Xiang, R., Cao, L., He, W., Liu, S., Shi, X., 2019. Geochemistry of core sediments along the Active Channel, northeastern Indian Ocean over the past 50,000 years: Sources and climatic implications. Palaeogeography, Palaeoclimatology, Palaeoecology 521, 151-160.

[36] McDonough and Sun., 1995. The composition of earth. Chemical Geology 120: 223-253.

[37] McLennan, S. M., Hemming, S., McDaniel, D. K., Hanson, G. N., 1993. Geochemical approaches to sedimentation, provenance, and tectonics. In: Special Papers-Geological Society of America 284, 21-40.

[38] Metang, V., Nomo, N. E, Ganno, S; Takodjou, W. J. D., Teme, M. A. E; Teda, S. A. C., Fossi. D. H., Mbakam, N. M. D., Tchameni, R., Nkoumbou, C., Nzenti, J. P., 2022. Anatexis of metadiorite from the Yaoundé area, Central African Orogenic Belt in Cameroon: implications on the genesis of in-source granodiorite leucosomes. Arabian Journal of geosciences 15, 359.

[39] Migdisov, A. A., 1960. On the titanium/aluminium ratio in sedimentary rocks. Geochemistry USSR. (English transl) 2, 178-194.

[40] Miyashiro, A., 1974. Volcanic rock series in island arcs and active continental margins. American Journal of Science 274, 321-355.

[41] Mukete, K. O., Minyem, D., Tamen, J., Nkoumbou. C., Fuh, C. G., Tchakounté Numbem, J. 2022. Petrology of ophiolites of Memel, Nsimè-Kellé and Mapan (Yaoundé group): Evidence of the geodynamic evolution of the Pan-African orogeny in South Cameroon. Journal of African Earth Sciences 191, 104537.

[42] Mvondo, H., Owona, S., Mvondo, O. J., Essono, J., 2007. Tectonic evolution of the Yaoundé segment of the Neoproterozoic Central African Orogenic Belt in Southern Cameroon. Canadian Journal of Earth Science 44 (4), 433-444.

[43] Nédélec, A., Macaudière, J., Nzenti, J. P., Barbey, P., 1986. Structural and metamorphic evolution of the Mbalmayo schists (Cameroon): implications for the structure of the Pan-African mobile belt of Central Africa, close of the Congo craton. Comptes Rendus de l'Academie des Sciences de Paris, Tome 303 (Series II): 75-80.

[44] Nesbitt, H., Young, G., 1984. Prediction of some weathering trends of plutonic and volcanic rocks based on thermodynamic and kinetic consideration. Geochimica Cosmochimica Acta 48, 1523-1534.

[45] Ngako, V., Njonfang, E., 2011. In: Damien Closson, Dr (Ed.), Plates Amalgamation and Plate Destruction, the Western Gondwana History. Tectonics. InTech 978-953-307545-7.

[46] Ngamy Kamwa, A., Tchakounte Numbem, J., Nkoumbou, C., Owona, S., Tchouankoue, J. P., Mvondo Ondoa, J., 2019. Petrology and geochemistry of the Yoro-Yangben Pan-African granitoids intrusion in the Archean Adamawa-Yade crust (Sw-Bafia, Cameroon). Journal of African Earth Sciences 150, 401-414.

[47] Ngnotué, T., Ganno, S., Nzenti, J. P., Schulz, B., Tchaptchet Tchato, D., Suh Cheo, E., 2012. Geochemistry and geochronology of Peraluminous High-K granitic leucosomes of Yaoundé series (Cameroon): evidence for a unique Pan-African magmatism and melting event in North Equatorial Fold Belt. International Journal of Geosciences 3, 525-548.

[48] Ngnotué, T., Nzenti, J. P., Barbey, P., Tchoua, F. M., 2000. The Ntui-Betamba high grade gneisses: A Northward extension of the Pan-African Yaoundé gneisses in Cameroon. Journal of African Earth Sciences 31, 369-381.

[49] Ngo Bidjeck, B. L. M., Betsi, B. T., Nga, M. Y. N. L., Belnoun, N. R. N., Molotouala, A. C., McFarlane, C., Bitom D. L., 2020. Geochemistry of rutile from the Pan-African Yaoundé metamorphic group: Implications for provenance and conditions of formation. Journal of African Earth Sciences 170, 103912.

[50] Nkoumbou, C., Barbey, P., Yonta-Ngouné, C., Paquette, J. L., Villiéras, D. F., 2014. Precollisional geodynamic context of the southern margin of the Pan-African fold belt in Cameroon. Journal of African Earth Sciences 99, 245-260.

[51] Nkoumbou, C., Yonta-Ngoune, C., Villiéras, F., Njopwouo, D., Yvon, J., Ekodeck, G. E., Tchoua, F., 2006. Discovery of ophiolite-related rocks in the Pan-African belt in Cameroon: Talc schists from Ngoung, Lamal Pougue, and Bibodi Lamal. Comptes Rendus Geoscience 338, 1167-1175.

[52] Nzenti, J. P., Barbey, P., Macaudière, J., Soba, D., 1988. Origin and evolution of the late Precambrian high-grade Yaoundé gneisses (Cameroon). Precambrian Research 38, 91-109.

[53] Olinga, J. B., Minyem, D., Mpesse, J. E., Ekodeck, G. E., 2010. Deformation history of Yaoundé Group in the Awae-Ayos area (Southern-Cameroon): Evidence for Pan-African thrust tectonics. Journal of the Cameroun Academy of Sciences 9 (1).

[54] Oliveira, E. P., Toteu, S. F., Araújo, M. N. C., Carvalho, M. J., Nascimento, R. S., Bueno, J. F., McNaughton, N., Basilici, G., 2006. Geologic correlation between the Neoproterozoic Sergipano Belt (NE Brazil) and the Yaoundé Belt (Cameroon, Africa). Journal of African Earth Sciences 44, 470-478.

[55] Oliveira, E. P., Windley, B. F., Araújo, M. N. C., 2010. The Neoproterozoic Sergipano orogenic belt, NE Brazil: A complete plate tectonic cycle in western Gondwana. Precambrian Research 181, 64-84.

[56] Oliveira, E. P., Windley, B. F., McNaughton, N. J., Bueno, J. F., Nascimento, R. S., Carvalho, M. J., Araujo, M. C., 2017. The Sergipano Belt. M. Heilbron et al. (eds.), São Francisco Craton, Eastern Brazil, Regional Geology Reviews 13, 241-254.

[57] Owona, S., Mvondo Ondoa, J., Ratschbacher, L., Ndzana, M. P. S., Tchoua, F. M., Ekodeck, G. E., 2011b. The geometry of the Archean, Paleo- and Neoproterozoic tectonics in the Southwest Cameroon. Comptes Rendus Geosciences 343, 312-322.

[58] Owona, S., Ratschbacher, L., Nsangou N. M., Muhammad, G. A., Mvondo Ondoa, J., Ekodeck G. E., 2021. How diverse is the source? Age, provenance, reworking, and overprint of Precambrian meta-sedimentary rocks of West Gondwana, Cameroon, from zircon U-Pb geochronology. Precambrian Research 359, 106220.

[59] Owona, S., Schulz, B., Ratschbacher, L., Mvondo Ondoa, J., Ekodeck, G. E., Tchoua, M. F., Affaton, P., 2011a. Pan-African metamorphic evolution in the Southern Yaoundé Group (Oubanguide Complex, Cameroon) as revealed by EMP-Monazite dating and thermobarometry and garnet metapelites. Journal of African Earth Sciences 59, 125-139.

[60] Penaye, J., 1988. Petrology and Structure of the Metamorphic Ensembles of South-East Poli (North Cameroon). Ph. D. thesis, INPL, Nancy, Unpublished.

[61] Penaye, J., Kröner, A., Toteu, S. F., Van Schmus, W. R., Doumnang, J. C., 2006. Evolution of the Mayo Kebbi region as revealed by zircon dating: An early (ca. 740 Ma) Pan-African magmatic arc in southwestern Chad. Journal African Earth Sciences 44, 530-542.

[62] Pin, C., Poidevin, J. L., 1987. U-Pb zircon evidence for a Pan-African granulite facies metamorphism in the Central African Republic. A new interpretation of high-grade series of the northern border of the Congo craton. Precambrian Research 36, 303-312.

[63] Roddaz, M., Debat, P., Nikiéma, S., 2007. Geochemistry of Upper Birimian sediments (major and trace elements and Nd-Sr isotopes) and implications for weathering and tectonic setting of the Late Paleoproterozoic crust. Precambrian Research. 159, 197-211.

[64] Ronov, A. B., Migdisov, A. A., 1971. Geochemical history of the crystalline basement and the sedimentary cover of the Russian and North American platform. Sedimentology, 16, pp. 137-185.

[65] Roser, B. P, Korsch, R. J., 1988. Provenance signatures of sandstone-mudstone suites determined using discriminant function analysis of major-element data. Chem Geol 67, 119-139.

[66] Roser, B. P., Korsch, R. J., 1986. Discrimination of tectonic setting of sandstone-mudstone suites using SiO_2 content and K_2O/Na_2O ratio. Journal of Geology 94, 635-650.

[67] Rudnick, R. L., Gao, S., 2013. Composition of the Continental Crust. Treatise on Geochemistry (2^{nd} ed.). Amsterdam: Elsevier.

[68] Saha-Fouotsa, A. N., Vanderhaeghe, O., Barbey, P., Eglinger, A., Tchameni, R., Zeh, A., Tchunte, P. F., Nomo, E. N., 2019. The geologic record of the exhumed root of the Central African Orogenic Belt in the central Cameroon domain (Mbé–Sassa-Mbersi region). Journal of African Earth Sciences 151, 286–314.

[69] Stendal, H., Toteu, S. F., Frei, R., Penaye, J., Njel, U. O., Bassahak, J., Nni, J., Kankeu, B., Ngako, V., Hell, J. V., 2006. Derivation of detrital rutile in the Yaoundé region from the Neoproterozoic Pan-African belt in southern Cameroon (Central Africa). Journal of African Earth Sciences 44, 443-458.

[70] Tarney, J., 1977. Petrology, mineralogy and geochemistry of the Falkland Plateau basement rocks, site 300, Deep Sea Drilling Project. Int. Rep. Deep Sea Drilling Project 36, 893-921.

[71] Taylor, H. P., 1979. Oxygen and hydrogen isotope relationships in hydrothermal mineral deposits. In: Barnes H. L. (Eds.), Geochemistry of hydrothermal ore deposits, 2 edition. Wiley, New York, 236-277.

[72] Taylor, S. R., McLennan, S. M., 1985. The continental crust: Its Composition and Evolution. Blaskwell Science, Oxford.

[73] Tchakounté Numben, J., Toteu, S. F., Van Schmus, W. R., Penaye, J., Deloule, E., Mvondo Ondoua, J., Houketchang, M. B., Ganwa, A. A., White, W. M., 2007. Evidence of ca.1. 6-Ga detrital zircon in the Bafia Group (Cameroon): Implication for the chronostratigraphy of the Pan-African Belt north of the Congo craton. Comptes Rendus Geoscience 339, 132-142.

[74] Tchakounté, J. N., Eglinger, A., Toteu, S. F., Zeh, A., Nkoumbou, C., Mvondo-Ondoa, J., Barbey, P., 2017. The Adamawa-Yade domain, a piece of Archean crust in the Neoproterozoic Central African Orogenic belt (Bafia area, Cameroon). Precambrian Research 299, 210-229.

[75] Toteu S. F, Michard A, Bertrand, J. M., Rocci, G., 1987. U/Pb of Precambrian rock from North-Cameroon, Orogenic evolution and chronology of the Pan-African belt of Central African. Precambrian Research 37, 71-87.

[76] Toteu, S. F., Penaye, J., Deloule, E., Van Schmus, W. R., Tchameni, R., 2006b. Diachronous evolution of volcano-sedimentary basins north of the Congo craton: Insights from U- Pb ion microprobe dating of zircons from the Poli, Lom and Yaoundé Groups (Cameroon). Journal of African Earth Sciences 44, 428-442.

[77] Toteu, S. F., Penaye, J., Djomani Poudjom, H. Y., 2004. Geodynamic evolution of the Pan-African belt in Central Africa with special reference to Cameroon. Canadian Journal of Earth Sciences 41, 73-85.

[78] Toteu, S. F., Yongue, R. F., Penaye, J., Tchakounte, J., Seme Mouangue, A. C., Van Schmus, W. R., Deloule, E., Stendal, H., 2006a. U-Pb dating of plutonic rocks involved in the nappe tectonic in southern Cameroon: consequence for the Pan-African orogenic evolution of the central African fold belt. Journal of African Earth Sciences 44, 479-493.

[79] Vicat, J. P., Moloto-A-Kenguemba, G., Pouclet, A., 2001. Granitoids of the Proterozoic cover of the Congo craton northern edge (South-East of Cameroon and South-West of the Central African Republic), witnesses of a post-Kibarian to pre-Pan-African magmatic activity Comptes Rendus de l'Academie des Sciences, Paris 332, 235-242.

[80] Vicat, J. P., Pouclet, A., Nkoumbou, C., Sémé Mouangué, A., 1997. The fissural Neoproterozoic volcanism of the lower Dja, Yokadouma (Cameroon) and Nola (RCA) series. Geotectonic meaning. Comptes Rendus de l'Academie des Sciences de Paris 325, 671-677.

[81] Yonta-Ngoune, C., 2010. Geological context of the Boumnyebel talcschists (Cameroun): Inferences on the Pan-African Belt of Central Africa. Ph.D. thesis, University of Yaoundé I: 221 p + annexes.

[82] Yonta-Ngouné, C., Nkoumbou, C., Barbey, P., Le Breton, N., Montel, J. M., Villiéras, F., 2010. Geological context of the Boumnyebel talcschists (Cameroun): Inferences on the Pan-African Belt of Central Africa. Comptes Rendus Geoscience 342, 108-115.